A review of phase change heat transfer in shape-stabilized phase change materials (ss-PCMs) based on porous supports for thermal energy storage

Shuai Zhang[a], Daili Feng[a], Lei Shi[a], Li Wang[a], Yingai Jin[b], Limei Tian[c], Ziyuan Li[c], Guoyong Wang[d], Lei Zhao[d], Yuying Yan[a,e,*]

a Fluids & Thermal Engineering (FLUTE) Research Group, Faculty of Engineering, University of Nottingham, Nottingham, NG7 2RD, UK

b State Key Laboratory of Automotive Simulation and Control, Jilin University, Changchun 130022, China

c Key Laboratory of Bionic Engineering (Ministry of Education), Jilin University, Changchun 130022, China

d Department of Materials Science and Engineering, Jilin University, Changchun 130022, China

e Research Centre for Fluids and Thermal Engineering, University of Nottingham Ningbo China, Ningbo 315100, China

* = corresponding author details, Yuying.Yan@nottingham.ac.uk

Abstract

Latent heat thermal energy storage (LHTES) uses phase change materials (PCMs) to store and release heat, and can effectively address the mismatch between energy supply and demand. However, it suffers from low thermal conductivity and the leakage problem. One of the solutions is integrating porous supports and PCMs to fabricate shape-stabilized phase change materials (ss-PCMs). The phase change heat transfer in porous ss-PCMs is of fundamental importance for determining thermal-fluidic behaviours and evaluating LHTES system performance. This paper reviews the

recent experimental and numerical investigations on phase change heat transfer in porous ss-PCMs. Materials, methods, apparatuses and significant outcomes are included in the section of experimental studies and it is found that paraffin and metal foam are the most used PCM and porous support respectively in the current researches. Numerical advances are reviewed from the aspect of different simulation methods. Compared to representative elementary volume (REV)-scale simulation, the pore-scale simulation can provide extra flow and heat transfer characteristics in pores, exhibiting great potential for the simulation of mesoporous, microporous and hierarchical porous materials. Moreover, there exists a research gap between phase change heat transfer and material preparation. Finally, this review outlooks the future research topics of phase change heat transfer in porous ss-PCMs.

Highlights:

1. The recent advances in experimental and numerical investigations on phase change heat transfer in porous ss-PCMs are reviewed.
2. Paraffin and metal foams are the mostly used PCM and porous support respectively in the experimental studies.
3. Compared to REV-scale simulation, the pore-scale simulation can provide extra flow and heat transfer characteristics in pores.
4. There exists a research gap between phase change heat transfer and material preparation.

Keywords:

shape-stabilized phase change materials;

porous supports;

phase change heat transfer;

thermal energy storage.

Word Count: 11623

1. Introduction

Renewable energy has been attracting increasing interest in the past decades due to its significant potentials for addressing growing energy demand and greenhouse gas emissions. According to “World Energy Outlook 2018” by International Energy Agency (IEA), the growing world economy and newly added 1.7 billion people are projected to push up global energy demand by 1/4 to 2040. And more energy-related CO2 will be emitted, which is estimated to exceed efforts taken to tackle climate change [1]. Renewable energy provides an attractive solution to alleviate growingly global energy demand and achieve a low-carbon future.

Among various renewable energy sources, solar energy continues to be a promising candidate to produce thermal energy for domestic applications, industrial manufactures and buildings. However, there is a temporal and geographic mismatch between thermal energy supply and demand. As a result, thermal energy storage (TES) is proposed to address this problem [2].

Currently, there are mainly three thermal energy storage technologies: sensible heat storage, latent heat storage and thermochemical reaction storage [3]. Table 1 summarizes the principle, advantages, typical materials and application areas of these TES technologies. As shown in this table, latent heat materials, or phase change materials (PCMs) has advantages of high energy storage density, high latent heat and the ability to maintain an almost constant temperature, and thus it is most widely used [4]. These advantages contribute to not only reduce equipment ability required and cost but also improve thermal storage performance. As a consequence, PCMs are most investigated among these three TES technologies [5].

Table 1

Principle, advantages, typical material and application areas of three TES technologies [6, 7]

TES technology	Principle	Advantage	Typical material	Application
Sensible heat storage	Increasing or decreasing the temperature of storage material	① Low cost ② Easy operation	Water, rock, concrete, liquid metals, etc	Solar energy storage Building structure
Latent heat storage	Phase transition of solid-liquid	① High energy storage density ② High latent heat ③ Maintaining an almost constant temperature	Paraffins, salt hydrates, metallics, etc	Solar engineering Heat pump Spacecraft thermal control Industrial waste heat storage
Thermochemical reaction storage	A reversible chemical reaction	① Highest energy storage density ② Negligible heat losses	Ammoniates, hydrates, metal hydrides, etc	No application currently

Nevertheless, pure PCMs suffer from two problems: low thermal conductivity ($\approx$ 0.1W m^{-1} K^{-1}) and leakage, which limits its utilization in many sectors [8]. For example, in some electronic devices, the chip generates heat transiently or periodically, which requires an efficient cooling system to dissipate heat. However, the poor conductivity of pure PCMs decreases the heat transfer rate and increases the possibility of chip exposure to an extremely high-temperature environment [9]. One of the solutions is integrating porous supports with PCMs to fabricate shape-stabilized phase change materials (ss-PCMs) [10]. According to the pore size, porous supports are classified as macroporous (>50nm), mesoporous (2~50nm), microporous (<2nm) and hierarchical porous (ranging from marco to micro) materials [11]. The widely-used support materials are shown in Fig.1. Different types of support materials have varying properties and functions: metal foams, a typical macroporous material, possess high thermal conductivity and thus are implemented as heat delivery promoter; due to the small pore and large surface area, meso- and microporous materials show a strong guest-host interaction and therefore avoid leakage; in hierarchical porous materials, macropores act as the cavity to store PCMs, mesopores provide transport pathway and micropores give capillary force to immobilize PCMs [12].

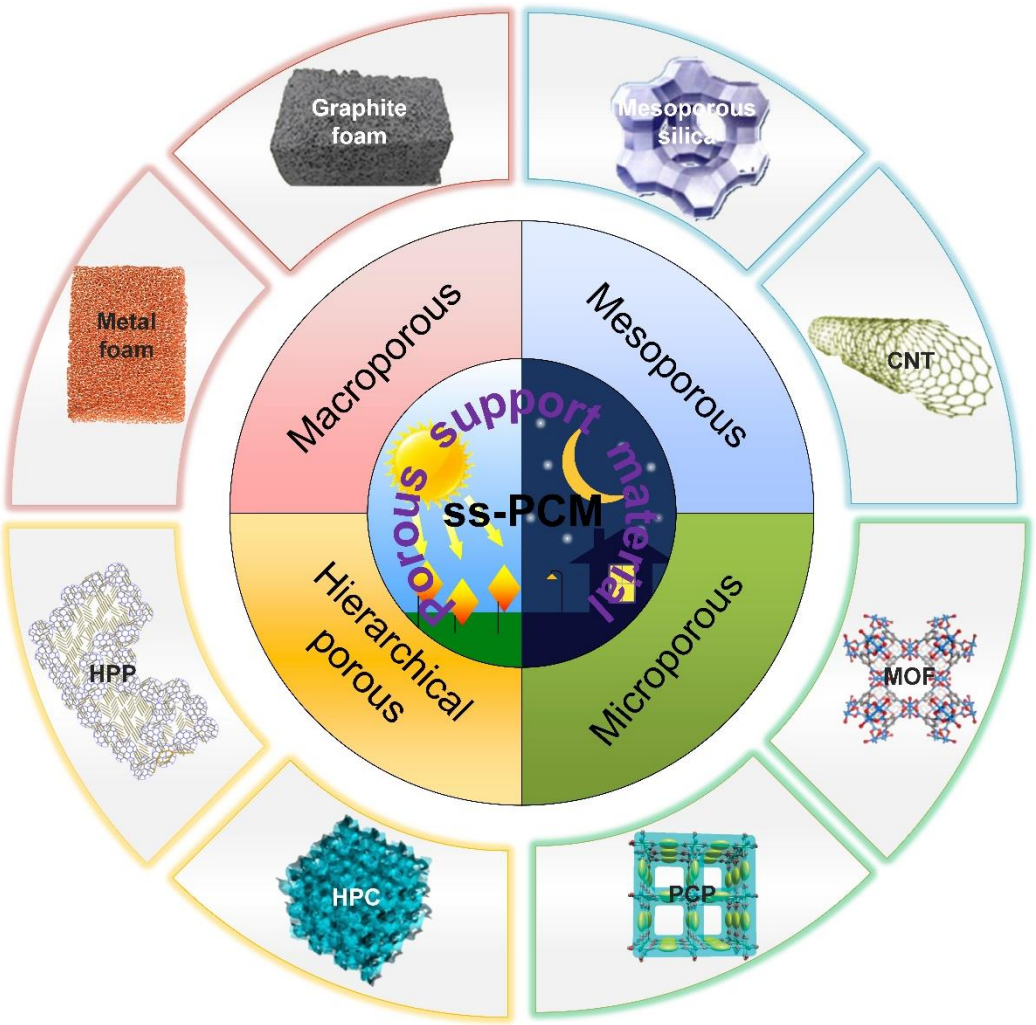

Fig.1. Porous support materials of ss-PCMs: graphite foam [13], mesoporous silica [12], carbon nanotube (CNT) [14], metal-organic framework (MOF) [12], porous coordination polymer (PCP) [15], hierarchical porous polymer (HPP) [16], hierarchical porous carbon (HPC) [17].

Many researchers have reviewed the progress on porous ss-PCMs. Rehman et al. [18] reported a review on heat transfer augmentation of PCMs using porous metal foams and carbon materials. Kenisarin et al. [19] introduced the fabrication of porous ss-PCMs with expanded materials such as perlite and vermiculite in their review paper. Umair et al. [13] reviewed researches on fabrication of porous shape-stabilized organic PCMs. Huang et al. [8] summarized the key studies on porous materials used as the supports of porous ss-CPMs. Feng et al. [11] presented a review on fabrication, characterization, enhancement and molecular simulation of nanoporous ss-PCMs.

Gao et al. [12] summarized recent studies on nanoconfinement effects on thermal properties of nanoporous ss-PCMs. Zhang et al. [5] reported a review on porous ss-PCMs fabricated by using metal foams and carbon materials, from the aspects of production, characterization, application as well as mathematical models describing phase change heat transfer in the composite PCMs. Phase change heat transfer is of remarkable importance for determining the thermal-fluidic behaviours and evaluating the performance of LHTES systems [20]. A good understanding of flow and heat transfer characteristics during the phase change process helps to realise the interactions between porous supports and PCM cores, and thus to design LHTES systems with higher loading, longer durability and higher thermal performance. A great number of researchers have carried out studies and significant advancements have been achieved on phase change heat transfer in porous ss-PCMs. However, to the best of our knowledge, there are very limited reviews on the solid-liquid phase-change heat transfer in porous ss-PCMs [5]. Since the phase change heat transfer in porous ss-PCMs has attracted increasing interest, this paper reviews the recent experimental and numerical progress on phase change heat transfer in porous ss-PCMs. Materials, methods, apparatuses and significant outcomes are presented in the section of experimental studies. Numerical advancements are introduced from aspects of different simulation methods, i.e. representative elementary volume (REV)-scale method and pore-scale method. Finally, future research topics are suggested.

2. Experimental study on solid-liquid phase-change heat transfer in porous ss-PCM

The major advantage of experimental studies is that they are able to provide “directly interpretable” and reliable results [21]. In addition, data collected from

experiments provide the validation source for numerical studies. Hence, a great number of experiments are performed by researchers to study the solid-liquid phase-change heat transfer in ss-PCMs based on porous supports.

2.1 Materials, methods and experimental apparatus in phase-change heat-transfer investigations

2.1.1 Materials and methods

To best of our knowledge, the first experimental investigation on the solid-liquid phase-change heat transfer of porous ss-PCM was conducted by Weaver and Viskanta in 1986 [22]. In their research, water and glass beads were employed as PCM and porous support, respectively. Since then, it has been over 30 years for investigations on phase-change heat transfer of porous ss-PCMs, and materials have changed a lot. Table 2 lists ss-PCMs and their properties in experimental investigations on solid-liquid phase-change heat transfer. Literature covers the first research in 1986 to the latest ones in 2019. Furthermore, Fig. 2. gives statistic of materials and properties of porous ss-PCMs employed. It can be seen that overwhelming researchers focus on low-temperature PCMs (the phase change point lower than 100℃ [5]). The only study on middle-temperature PCM was carried out by Zhang et al. where the melting temperature of PCM was 218-228℃ [23]. In addition, the pore size of porous supports employed in all researches is over 0.1mm. In other words, all the ss-PCMs investigated are macroporous. Experimental studies on phase change heat transfer in mesoporous, microporous and hierarchical porous ss-PCMs have yet been conducted.

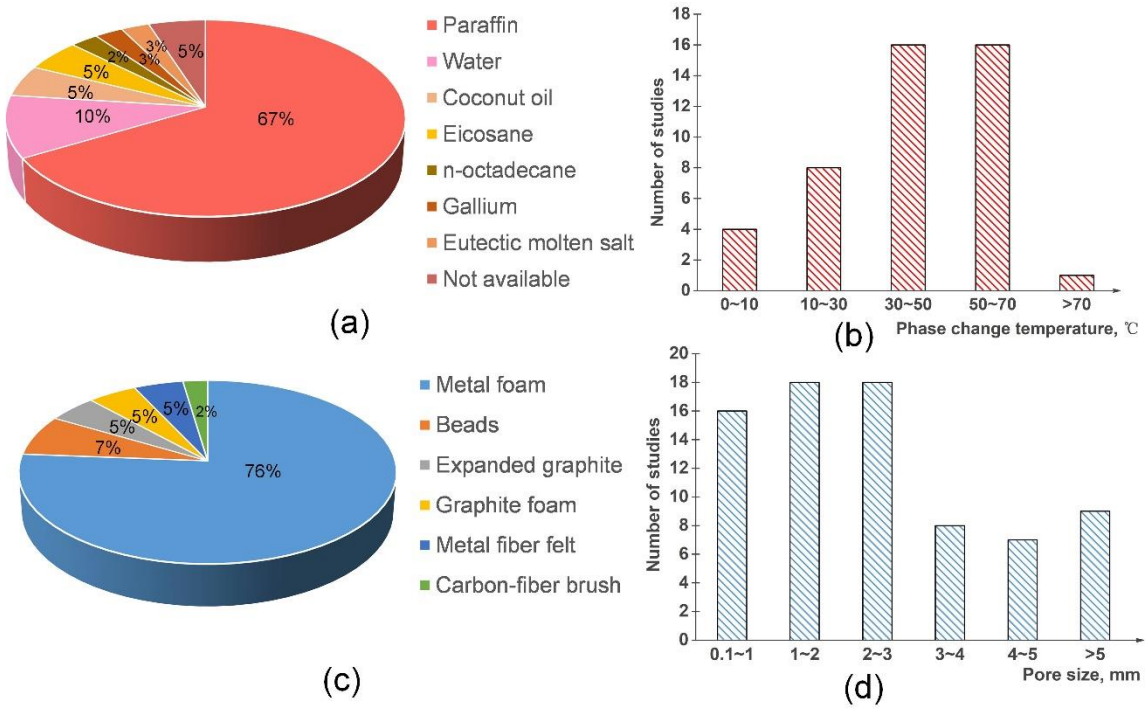

Fig. 2. Statistic of ss-PCMs and properties employed in investigations on phase change heat transfer: (a) types of PCMs (b) number of studies under different PCMs phase change temperature (c) types of porous supports (d) number of studies under different pore sizes

The metal foam is the most used porous support in the experimental studies. There are mainly two methods to fabricate metal foam based ss-PCMs. The first one is the directly pouring method, which is adopted by Righetti et al. [24], Mallow et al. [25], etc. The procedure of this method is that the hot liquid PCM is directly poured into a container and mixed with the porous support. This approach is simple and does not need extra equipment, however, due to the air existing in the porous support, liquid PCM cannot infiltrate the support completely. Thus more researchers employed the vacuum impregnation (or vacuum infiltration) method, such as Zhang et al. [20], Jin et al. [26], etc. A typical flow chart is presented in Fig. 3. The procedure consists of six steps: firstly, the solid PCM, metal foam and a mesh which is used to support the foam are placed into a container. A vacuum pump is connected to the container and

switched on to evacuate the air. Secondly, the container is heated and the metal foam sinks into the molten PCM. After the porous support is fully impregnated by liquid PCM, the heating process is ended and the vacuum pump is switched off at the same time. Then the container is cooled. When the PCM is completely solidified, the container is reheated slightly to make it easy to withdraw the specimen. Finally, the composite PCM is taken out and the surplus PCM on the surface is removed.

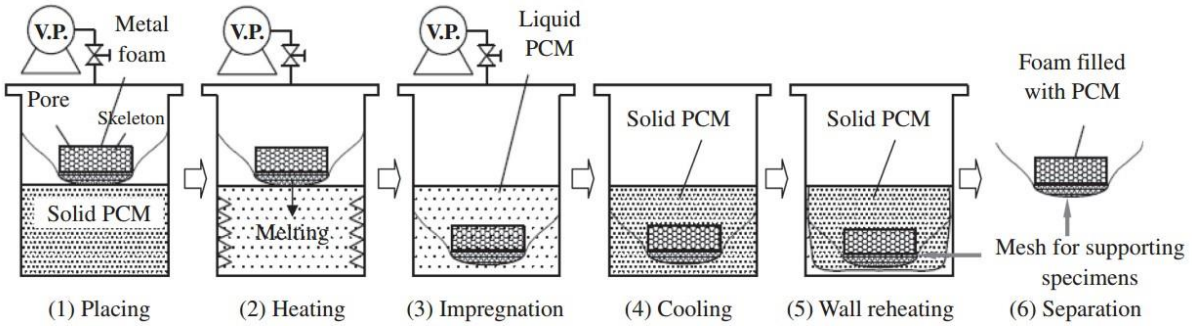

Fig. 3. Flow chart of vacuum impregnation method to fabricate metal foam based ss-PCM [27] (V.P. represents vacuum pump)

Table 2

Summary of porous ss-PCMs and their properties in experimental studies on phase change heat transfer

Ref.	PCM/porous support	Porosity	Pore size (mm)	Phase change point of PCM (℃)	Latent heat of PCM (J/g)
[22]	Water/glass beads	0.36-0.38	-	0	-
[28]	Water/aluminum beads	0.39	-	0	-
[29]	Gallium/glass beads	0.385	-	29.78	-
[30]	Paraffin/copper foam	0.90-0.95	0.85-2.54	58	181
[31]	Paraffin/aluminum foam	0.9137	2.82	55-60	120
[32]	PureTemp® 25/aluminum foam PureTemp® 25/copper foam PureTemp® 25/graphite foam	0.921-0.933 0.947 0.811	1.27-5.08 1.27 0.42	24.1-26.3	187
[33]	Water/aluminium foam	0.946	0.64	0	315-333
[34]	Paraffin/aluminium foam	0.77-0.95	-	50-60	117
[35]	Paraffin/aluminium foam	0.859-0.958	-	52-57	200
[36]	Paraffin/copper foam	0.95	5.08	48.4-63.6	148.8
[37]	Paraffin/carbon-fiber brushes	0.992-0.9932	-	40-53	180
[38]	PCM/ aluminium foam	-	2.54	15	182
[39]	Water/copper foam	0.93-0.97	0.85-3.18	0	-

[40]	Paraffin/copper fiber sintered felt	0.75-0.95	0.15	48.6	217.9
[41]	Paraffin/copper foam	0.968	1.27	48-50	250
[42]	Coconut oil/ aluminium foam	0.88-0.96	5.08	24	103
[43]	Paraffin/copper foam	0.96	1.27	-	-
[44]	Paraffin /stainless-steel fiber felt	0.8-0.9	0.1-0.2	47.38	170.7
[45]	Paraffin/ aluminium foam	0.92-0.93	0.635-5.08	42-64	165-250
[46]	Coconut oil/ aluminium foam	0.88-0.96	1.27-5.08	24	103
[47]	Eicosane/copper foam	0.95	0.127-2.54	36.5	-
[9]	Paraffin/copper foam	0.90-0.98	0.64-2.54	46.48-60.39	102.1
[20]	Paraffin/copper foam	0.97	1.02	54.43-64.11	175.24
[48]	Paraffin/copper foam	0.92	1.27	48-50	136.4
[49]	Paraffin/copper foam $CaCl_2{\cdot}6H_20$/copper foam Paraffin/expanded graphite	0.815, - 0.815 -	0.847 0.847 -	25-28, 29 25-28	184 190.8 184
[25]	Paraffin/aluminium foam PT37/aluminium foam Paraffin/graphite foam	0.905-0.912 0.905-0.912 -	0.635-2.54 0.635-2.54 -	55.2 37 55.2	132.2 210 132.2
[23]	NaNO3 and KNO3/copper NaNO3 and KNO3/nickel foam	0.965 0.975	2.54 2.54	218-228 218-228	122.89 122.89
[50]	Paraffin/copper foam	0.97	2.54	68	213
[51]	Paraffin/copper foam	0.98	1.69	52-54	-

[26]	Paraffin/copper foam	0.949-0.961	0.51-1.69	46.4	-
[52]	Paraffin/copper foam	0.95	0.635-5.08	52-60	-
[53]	Paraffin/ aluminium foam	0.7-0.9	-	46-52	-
[54]	Paraffin/expanded graphite	-	-	61.33-61.62	170.7-180.6
[55]	Paraffin/copper foam	0.974	2.54	26	179
[24]	Paraffin/ aluminium foam	0.893-0.948	0.635-5.08	40	165
[56]	n-octadecane/aluminium foam	0.87-0.96	0.635-5.08	28	243.5
[57]	Paraffin/copper foam	0.95-0.97	0.73-1.69	47-57	167
[58]	N-eicosane/copper foam	0.86	2.54	36.5	-
[59]	Paraffin /copper foam	0.91	2.54-5.08	35	230

2.1.2 Experimental apparatus

The experimental apparatus is relatively simple in early researches. For example, Weaver et al. [22] just employed a conventional camera to study the freezing process of water. Later, more and more high-tech measurement devices are utilized to investigate the solid-liquid phase-change heat transfer in porous ss-PCMs. Table 3 gives a summary of the measurement device and type of measured data in literature from 1986 to 2019. An example of experimental apparatus is also shown in Fig. 4.

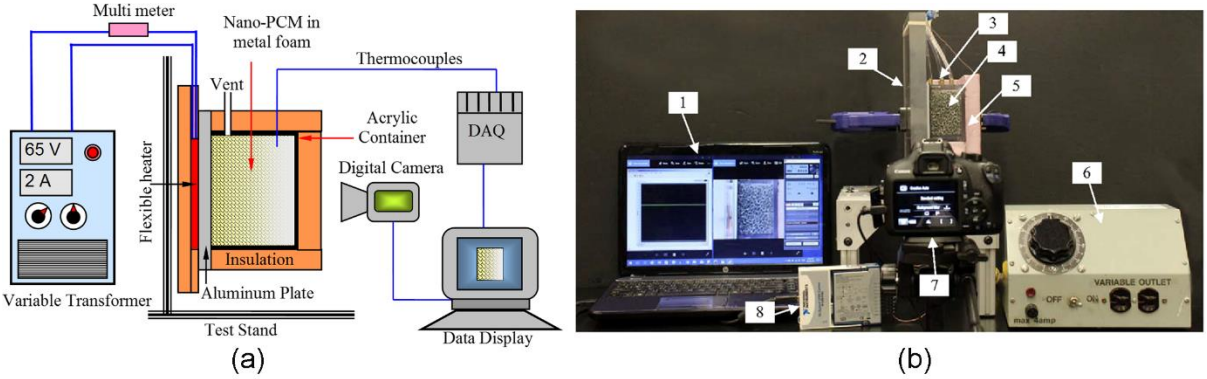

Fig. 4. Example of experimental apparatus for investigating phase-change heat-transfer process of porous ss-PCM: (a) schematic (b) photograph (1 – data display, 2 – test stand, 3 – vent, 4 – enclosure, 5 – insulation, 6 – variable transformer, 7 – digital camera, 8 – DAQ) [42]

Generally, temperature and solid/liquid interface are two commonly monitored parameters. To record the temperature variation, the thermocouple is used by most researchers, as Table 3 shows. Thermocouples are inserted into the ss-PCM and linked with data acquisition. Hence, the temperature at selected points can be monitored. The number of thermocouples varies in different researches. To our best knowledge, Martinelli et al. [59] employed the maximum number of thermocouples, 40, to investigate the phase-change heat-transfer process in a 400mm tube-and-shell test rig. Most researchers utilized thermocouples to monitor the temperature variation of PCM. However, since there is an apparent difference in thermal-physical properties between porous supports and PCM, the temperature of the two components may be

not the same [60]. To explore this thermal phenomenon, Zhang et al. [20] built a set of experimental apparatus where two T-type thermocouples were set into the ss-PCM. One was inserted into PCM in the support material pore to record the PCM temperature, while the other was soldered on the metal skeleton surface to measure the skeleton temperature. This experimental setup is first built by Zhang et al. [20] and it can be employed to experimentally investigate the local thermal non-equilibrium and provide data for the comparison with simulation results. However, the thermocouple has an intrinsic disadvantage: it only records the temperature variation at certain points, rather than the whole temperature field. To solve this problem, Jackson et al. [32], Zhang et al. [20] and Yao et al. [55] applied the infrared camera to capture the evolution of the whole temperature field.

With regard to the phase interface, the conventional camera was widely utilized to capture the solid/liquid interface. Some researchers also employed a high definition (HD) camera to obtain higher quality images [36, 41, 48, 55]. After images of phase interface being processed, some other parameters, such as melting/solidification fraction and rate, can be obtained. It is noteworthy that Chen et al. [31] employed an optical microscope to study the melting evolution of PCM at the pore scale, which provided new insights into the measurement of phase interface.

Table 3

Summary of measurement device and type of measured data in experimental studies on phase change heat transfer in porous ss-PCMs

Ref.	Measurement device	Type of measured data
[22]	Conventional camera	Phase interface
[23]	Thermocouple	Temperature variation of PCM at six positions
[28]	Thermocouple	Temperature variation of PCM at three positions
[29]	Thermocouple	Temperature variation of PCM at thirty-three positions
[30]	Thermocouple	Temperature variation of PCM at four positions
[31]	Infrared camera, microscope	Phase interface of melting process, temperature field of ss-PCM
[32]	Thermocouple, infrared camera	Temperature variation of PCM at four positions, temperature field of ss-PCM
[33]	Thermocouple	Temperature variation at inlet/outlet
[34]	Thermocouple, conventional camera	Average temperature variation, phase interface of melting process
[35]	Thermocouple, conventional camera	Phase interface
[36]	Thermocouple, HD camera	Temperature variation of PCM at three positions, phase interface, melting time
[37]	Thermocouple	Temperature variation of PCM at three positions
[38]	Thermocouple	Temperature variation of PCM at the axis
[39]	Thermocouple, conventional camera	Phase interface of solidification process, temperature variation of PCM at four positions, solidification fraction versus time, phase change time

[40]	Thermocouple	Temperature variation of PCM at three positions
[41]	Thermocouple, HD camera	Phase interface of melting process, temperature variation of PCM at fifteen position, phase change time, melting fraction
[42]	Thermocouple, conventional camera	Phase interface of melting process, temperature variation of PCM at one position, phase change time, melting fraction
[44]	Thermocouple, conventional camera	Phase interface of melting process, variation of surface temperature, phase change time
[45]	Thermocouple, conventional camera	Phase interface of melting process, temperature variation of heating wall and PCM at three positions, phase change time
[46]	Thermocouple, conventional camera	Phase interface of melting process, melting time
[47]	Thermocouple	Phase interface of melting/solidification process, temperature variation of PCM at one position
[9]	Thermocouple	Temperature variation of PCM at five positions
[20]	Thermocouple, infrared camera, conventional camera	Temperature of both PCM and skeleton at centre position, phase interface, temperature field of ss-PCM, phase change time
[48]	Thermocouple, HD camera	Temperature variation of PCM at nine positions and inlet/outlet, phase interface, melting time
[49]	Thermocouple	Temperature variation of PCM at three points and heater
[25]	Thermocouple	Temperature variation of PCM at two points and heater
[50]	Thermocouple	Temperature variation of PCM at six positions
[51]	Infrared camera, thermocouple	Temperature field of ss-PCM, temperature variation of PCM at two positions, phase change time
[26]	Infrared camera, thermocouple	Temperature field of ss-PCM, temperature variation of PCM at two positions, phase change time

[52]	Thermocouple, conventional camera	Temperature variation of PCM at five positions, phase interface of melting process, phase change time
[53]	Thermocouple	Temperature variation of PCM at nine positions
[54]	Thermocouple	Temperature variation of PCM at fifteen positions
[55]	Thermocouple, HD camera, infrared camera	Temperature variation of PCM at five positions, Temperature field of ss-PCM, phase interface of melting process, phase change time
[24]	Thermocouple	Temperature variation of PCM
[56]	Thermocouple	Temperature variation at fifteen points
[57]	Thermocouple	Temperature variation of PCM at eight points and heater
[58]	Thermocouple	Temperature variation of PCM at four points and heater
[59]	Thermocouple, conventional camera	Temperature variation of PCM at forty points and inlet/outlet, phase interface of melting/solidification process, phase change time

2.2 Solid-liquid phase-change process

2.2.1 Phase interphase evolution

In 2012, Li et al. [9] experimentally studied the melting process of paraffin enhanced by copper foam in a 100mm(length) x 45mm(width) x 100mm(height) rectangular cavity. The ss-PCM was heated on the left side. The solid/liquid interface at 3600s and 3780s presented a sloped shape. Later, they investigated the melting behavior of paraffin with porous stainless-steel fiber felt [44]. A mush region was observed under condition of 0.8 porosity. Zhang et al. [20] conducted an experiment to study the melting phase change in paraffin/copper foam composite ss-PCM. They found that at the initial stage, the melting front was almost parallel to the heating boundary, indicating that the heat conduction dominated the phase change heat transfer. With time elapsed, more PCM melted and the hot liquid PCM flowed upwards driven by buoyancy, leading to the upper PCM melting faster. As a result, the melting front became slope-shaped. A similar phenomenon can be found in Al-Jethelah et al. [42]'s research and the results are shown in Fig. 5. Al-Jethelah et al. classified the melting process into three stages according to the heat transfer mechanism:

(1) conduction-dominated stage: the melting interface was parallel to the heating wall and the thermal energy was transferred to solid PCM in the form of sensible heat (Fig. 5(b)).

(2) conduction-convection-mixed stage: liquid PCM flowed upwards due to the buoyancy force and a wide circulatory region was formed in the upper part, curving the interface; in the lower part, the interface was still vertical due to the conduction (Fig. 5(c), (d)).

(3) convection-dominated stage: With time elapsed, more PCM melted and was pushed by buoyancy force to flow upwards along the heating wall and downwards

along the solid/liquid interface. Thermal energy in hot liquid PCM was released during the downward flow process. More energy was absorbed by the upper part of interface, leading to a larger melting region at the upper, and thereby forming a more sloped interface (Fig. 5(e)-(g)).

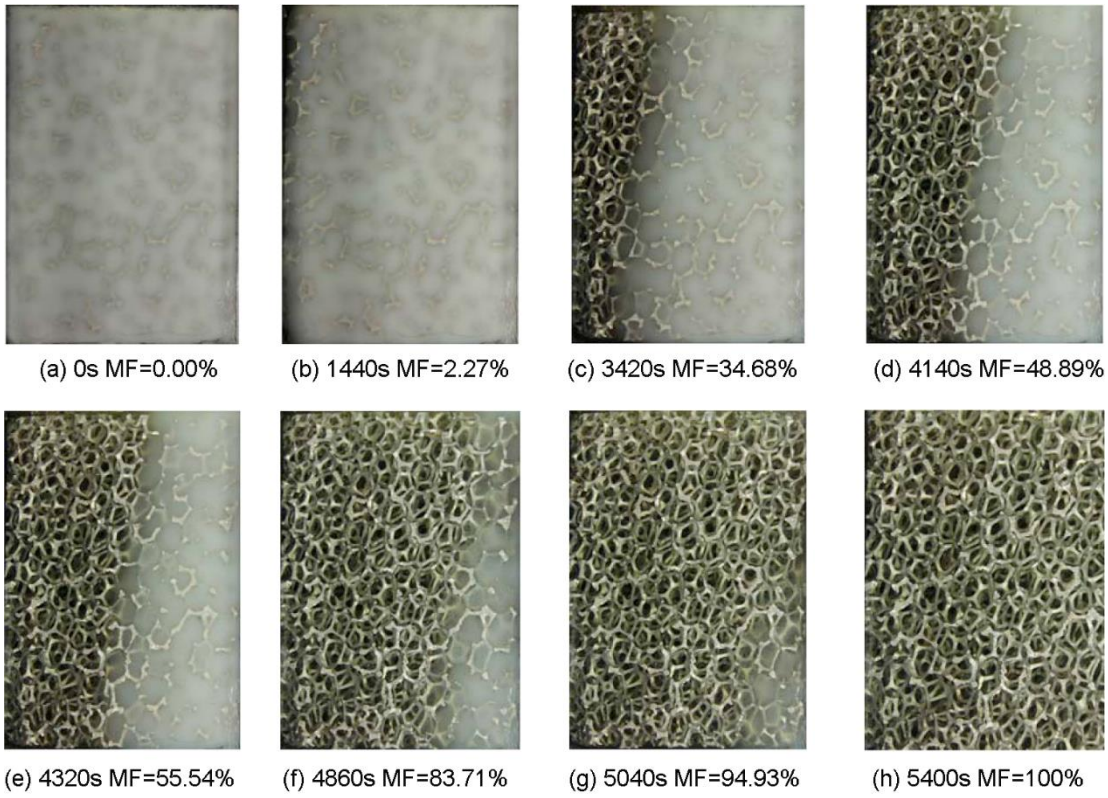

Fig. 5. Evolution of solid/liquid phase interface under the condition of left heated wall (MF: melting fraction) [42]

Diani et al. [45] used three kinds of paraffin with different melting temperatures as PCM and aluminium foam as porous support to study the phase change heat transfer in a 20mm(length) x 100mm(width) x 100mm(height) cavity. Venkateshwar et al. [46] investigated the melting process of aluminium foam/ coconut oil with CuO nanoparticles. The solid/liquid interface evolution obtained by these researchers is similar to that by Al-Jethelah et al. [42].

It should be noted that the above researches are under the condition of the left heating wall. Different heating position may lead to different solid/liquid interface. To

explore the mechanism, Zheng et al. [36] conducted an experiment where the paraffin/copper foam ss-PCM was heated by the left, bottom, and top wall, respectively. The interface propagation in the case of left heating wall was similar to Al-Jethelah et al. [42]'s results, while the other two cases were different. For the condition of the bottom heating wall, the melting front at the early stage was parallel to the heating boundary. However, at 4.5h, the PCM in the middle melted faster than on both sides because of the natural convection, and two symmetrical annular flows occurred. For the case of top heating, the phase interface was always parallel to the heating wall because the influence of natural convection was relatively insignificant.

The cylindrical container is another widely used enclosure for porous ss-PCMs [61]. In 2008, Siahpush et al. [47] investigated the melting/solidification process of eicosane/copper foam composite PCM in a 155.5mm(inner diameter) x 304.8mm(height) copper tube. During the test process, the outer wall temperature of the container was kept constant. 81 thermocouples were employed to monitor temperature variation. It was found that the curvature of solid/liquid interface in the case of metal foam was not as pronounced as the case of without metal foam because the metal foam enhanced the effective conductivity of ss-PCMs. Yang et al. [48] studied the phase change process in a tube-and-shell unit. Copper foam with/without a bottom fin was compounded into the paraffin to enhance heat transfer. For the PCM with copper foam, the interface was cone-shaped and developed from the inside to outside, while for the case with copper foam and bottom fin, the melting interface was inversed funnel-shaped. Recently, Yang et al. [41] performed a visual experiment to investigate the melting process of PCM/metal foam in a tube-and-shell unit. The solid/liquid interface propagation is presented in Fig. S1. It was found that at the initial stage (60min), the inner interface was vertical, indicating that the conduction

dominated the heat transfer. With the elapse of time, more PCM melted and the natural convection remarkably contributed to the heat transfer. The hot molten PCM was pushed upwards by buoyancy force and accelerated the phase change in the upper region, thereby forming a funnel-shape interface after 60min. For the outer solid/liquid interface, it was horizontal during the whole phase change process.

2.2.2 Temperature distribution and variation

Thermocouples are widely utilized to record temperature distribution and variation during the phase change process. For instance, Zhou et al. [49] arranged four thermocouples at different positions in a rectangular cavity. They found that by adding copper foam into paraffin, the heater temperature was reduced dramatically; during the melting process, the temperature of PCM with metal foam was higher than that without metal foam, implying that the heat was conducted to PCM faster with the assistance of metal foam. Mancin et al. [52] investigated the solid-liquid phase-change process of paraffin/copper foam composite ss-PCM. A lower surface temperature was observed compared with no-foam case. Wang et al. [53] studied the paraffin/aluminum foam composite ss-PCM in a Li-on battery. Their results showed that the existence of aluminum foam improved the temperature uniformity of PCM. Zhang et al. [23] experimentally investigated the phase change process of eutectic salt in a metal foam. Thermocouples were fixed along the axis and wall of a cylindrical container (see Fig. 6(a)). During the test procedure, the container was heated in the thermostatic oil bath. The temperature variation is shown in Fig. 6(b). For the pure PCM, the temperature at point D was higher than that at point B and C, while for copper foam/salt composite, the temperature at point B was highest. This is because the natural convection dominated the melting process of pure PCM while it was suppressed in the case of copper foam/salt composite.

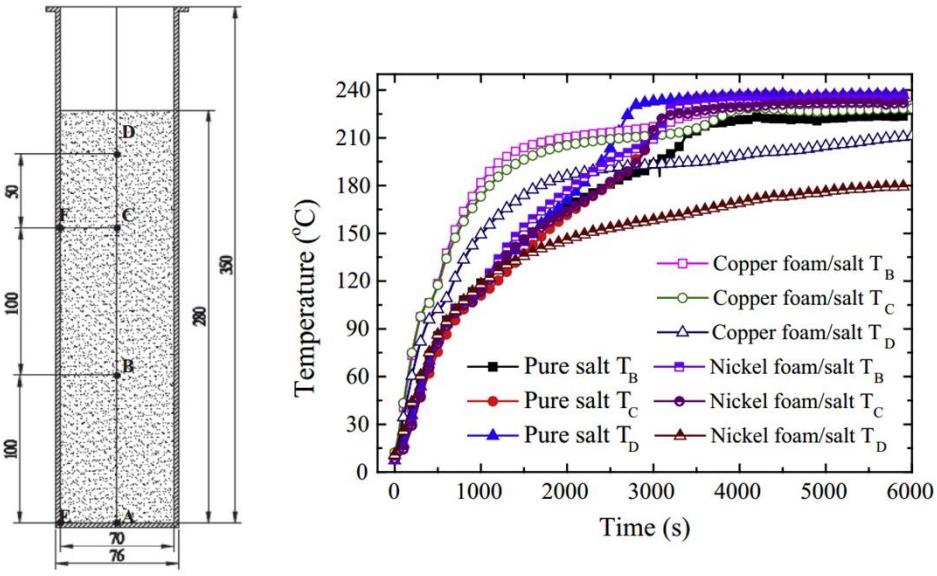

Fig. 6. Schematic of thermocouple arrangement (a) and temperature variation during melting process [23]

Recently, the infrared camera was used by some researchers to capture the entire temperature field. In Zhang et al. [20]'s experiment, the cavity was heated by the left wall and the results was presented in Fig.7. It can be seen that at the initial stage, the temperature contours were almost vertical, indicating that the heat conduction dominated the heat transfer. With the elapse of time, more PCM melted and the local natural convection became gradually notable, which accelerated the interface propagation in the top domain. The trend of temperature fields was similar to that of the solid/liquid interface in Fig. 5. In Fan and Jin's research, an infrared camera was equipped to record the temperature field during the melting process [51]. It was found that the temperature difference between the porous support and PCM became more pronounced as the phase change proceeded. Yao et al. [55] investigated the melting process of paraffin/copper foam with the assistance of an infrared camera. Their results showed that the copper foam improved the temperature distribution uniformity and increased the melting rate by 2 times.

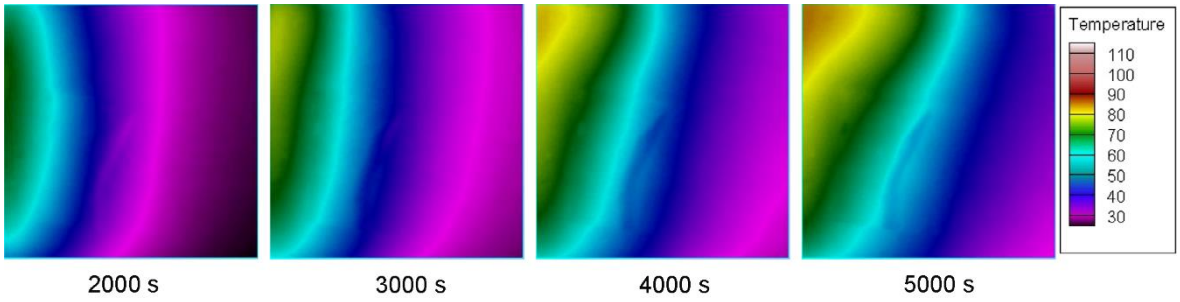

Fig. 7. Variation of temperature field captured by an infrared camera [20]

2.2.3 Comparison with pure PCM

The temperature field of PCM with/without metal foam is presented in Fig. 8. It can be seen that after adding the metal foam, the heat can be transfer effectively to the region away from the heating source and the temperature distribution is more uniform. It is generally believed that the addition of porous media promotes the heat conduction while it hampers the natural convection [18, 53]. The effects of the two aspects on the phase-change process are the opposite. Table 4 lists outcomes of adding porous media into PCM. All the researches illustrate that the phase change heat transfer is enhanced by porous support, indicating that the improvement of heat conduction is more prominent than the suppression of natural convection.

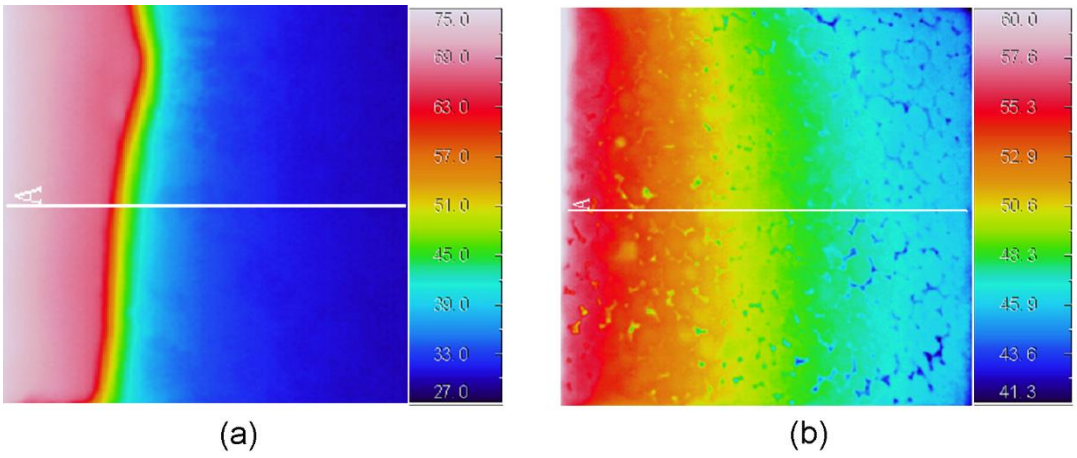

Fig. 8. Temperature field captured by the infrared camera (a) pure PCM (b) PCM with metal foam (the heating wall is placed on the left side) [31]

Table 4

Thermal performance of porous ss-PCM compared with pure PCM

Ref	PCM/porous support	Container	Outcomes
[39]	Water/copper foam	*l*: 28mm, *w*: 68mm, *h*: 68mm, Rectangular cavity	Total solidification time was saved 87.5% and 76.7% for metal foam with porosity of 0.93 and 0.97, respectively.
[42]	Coconut oil/aluminium foam	*l*: 50mm, *w*: 62mm, *h*: 72mm, Rectangular cavity	Melting process was improved by 41.2% at 1814W/m^2 and 2160s; Energy storage rate was increased by 28.81% at 2835W/m^2 and 2280s.
[45]	Paraffin/ aluminium foam	*l*: 20mm, *w*: 100mm, *h*: 100mm, Rectangular cavity	The total melting time was shorted by 50%.
[36]	Paraffin/copper foam	*l*: 100mm, *w*: 30mm, *h*: 100mm, Rectangular cavity	The total melting time was shortened 20.5%. The biggest temperature difference was reduced from 57℃ to 23℃.
[53]	Paraffin/ aluminium foam	*l*: 90mm, *w*: 50mm, *h*: 40mm, Rectangular cavity	The heat storage time was saved 26.4% and 25.6% in cases of heat flux = 7000W/m^2 and 12000 W/m^2, respectively.
[55]	Paraffin/ copper foam	*l*: 50mm, *w*: 5mm, *h*: 7mm, Rectangular cavity	Melting rate was improved by 2 times.
[49]	Paraffin, $CaCl_2 \cdot 6H_20$ /copper foam	80mm x 50mm x 30mm, Rectangular cavity	Effective thermal conductivities were improved by 1 and 2 times for paraffin and calcium chloride hexahydrate, respectively.
[41]	Paraffin/copper foam	*od*: 85mm, *id*: 22mm, *h*: 300mm Tube-and-shell unit	Melting time was shortened by 64%.
[48]	Paraffin/copper foam	*l*: 120mm, *w*: 60mm, *h*: 240mm, *id*: 20mm Tube-and-shell unit	Melting time was shortened by over 1/3.
[43]	Paraffin/copper foam	*od*: 126mm, *id*: 25mm, *h*: 325mm Tube-and-shell unit	Heat transfer rate was increased by 36%.
[33]	Water/aluminium foam	*id*: 177.8cm, *l*: 508cm 27 heat transfer tube: od: 0.64mm Tube-and-shell unit	The overall heat transfer coefficient was increased 20% for solidification process and 100% for melting process.

[23]	Entactic salt/ copper and nickel foam	*id*: 70mm, Tube	Solidification time was decreased by 28.8% and 19.3% in cases of copper foam and nickel foam, respectively.
[47]	Eicosane/copper foam	*id*: 155.5mm, *h*: 304.8mm, Tube	The effective thermal conductivity was increased from 0.423 W/ (m·K) to 3.06 W/(m·K); Consuming time was reduced from 375min to 85min for solidification process, and from 500min to 250min for melting process.
[24]	Paraffin/ aluminium foam	*od*: 62mm, *h*:800mm Tube	The time of melting/solidification was shortened by more than 2h.

2.2.4 Effect of porous support configuration

The porous support configuration, i.e. porosity and pore density, has a remarkable effect on phase change heat transfer characteristics of porous ss-PCMs. Many researchers conducted experiments to explore it. A summary of relevant studies is given in Table 5. The heat transfer enhancement is characterized using different parameters, such as melting/solidification rate, temperature distribution uniformity, decrease in base temperature, etc. All the researches illustrate that the decrease in porosity enhances the phase change heat transfer because a small porosity indicates a large high-thermal-conductivity volume in porous ss-PCMs, thereby improving the whole heat conductivity capacity of ss-PCM.

In contrast, the effect of pore size varies in different researches. As Table 5 shows, the small pore size improved the thermal performance of porous ss-PCM in Zhao et al. [30] and Mallow et al. [25]'s researches, while it had the negative effect in Li et al. [9] and Allen et al. [56]'s studies. The influence of pore size is attributed to two aspects: on the one hand, the decrease of pore size enhances the thermal conduction because it leads to a larger interactive surface area between PCM and support material; on the other hand, it hampers the natural convection of molten PCM because smaller pores limit the motion of liquid PCM. The two aspects compete and the final result is determined by the more significant one. The mechanism can be explained by Jin et al. [26]'s experiment. At 20℃wall superheat, the influences of the two aspects are equal, and thus the melting rates are the same. When the wall superheat is increased to 30℃, the natural convection is more intensive and the confine on convection exerted by small pores is more obvious. Hence, the melting rate in the case of 50PPI becomes smaller than that of 30PPI.

Table 5

Effects of porous support configuration on phase change heat transfer

Ref.	PCM/porous support	Outcomes
[57]	Paraffin/copper foam	Decrease in base temperature: 0.95ε* > 0.97ε
[39]	Water/copper foam	Solidification rate: 0.93ε > 0.97ε
[24]	Paraffin/aluminium foam	Phase change rate: 0.89ε > 0.93ε > 0.95ε
[34]	Paraffin/aluminium foam	Rate of PCM temperature variation: 0.77ε > 0.95ε
[9]	Paraffin/copper foam	Temperature distribution uniformity: 0.90ε > 0.95ε 10PPI > 40PPI
[56]	n-octadecane/aluminium foam	Phase change rate: 0.870ε > 0.912ε > 0.949ε Solidification rate: 20PPI > 40PPI
[30]	Paraffin/copper foam	Temperature difference between PCM and support: 0.85ε < 0.95ε 30PPI < 10PPI
[25]	Paraffin/aluminium foam	Melting rate: 40PPI > 20PPI > 10PPI
[26]	Paraffin/copper foam	Melting rate: 30PPI > 50PPI, 30℃ wall superheat 30PPI = 50PPI, 20℃ wall superheat
[46]	Coconut oil/ aluminium foam	Thermal energy storage rate: 20PPI > 5PPI > 10PPI, 0.00%~0.12%wt nanoparticles 5PPI > 20PPI > 10PPI, 0.3%wt nanoparticles

*: 0.95ε represents 0.95 porosity.

2.2.5 Effect of other configurations

2.2.5.1 Container inclination

Optimizing the container inclination may be an effective approach to enhance the phase change heat transfer of porous ss-PCM without consuming additional material and energy. To explore the effect of container inclination, Baby et al. [58] built a rotatable tracking mechanism where an 80mm x 62mm x 25mm heat sink filled with n-eicosane/copper foam composite PCM was mounted. The ss-PCM was heated by a bottom plate heater and the inclination ranged from 0° to 210°. However, they found that the inclination did not have remarkable influence on the phase change heat transfer of the porous ss-PCM. Later, Allen et al. [62] investigated the effect of inclination in a cylindrical closure. It was found that, for the PCM enhanced by heat pipe and metal foam, the average difference of liquid fraction between horizontal and vertical configurations was 0.05 and 0.01 for the melting and solidification process, respectively. Yang et al. [63] experiments were carried out at angles of 0°, 30°, 60°, and 90°. Their results showed that, for the pure PCM, the total melting time was saved 12.28%, 22.81% and 34.21% at 0°, 30° and 60, compared with the case at 90°. However, for PCM/metal foam, the effect of container inclination was neglectable. There also exists a different finding. Martinelli et al. [59] utilized a tube-and-shell test rig with a length of 400mm and found that the total solidification time was 1020s and 880s in cases of horizontal configuration and bottom-injection vertical configuration respectively, while the melting time was 820s and 810s.

2.2.5.2 Heat transfer fluid

To explore the effects of heat transfer fluid (HTF) temperature and flow rate, Yang et al. [48] designed a vertical tube-and-shell TES unit with a length of 24cm. Their results showed that when the HTF inlet temperature rose from 75℃ to 85℃, the time

was saved 63 mins for a selected point to rise from starting melting temperature to the ending temperature, while the time was shortened only about 10min when the HTF flow rate increased from 0.2m^3/h to 0.6m^3/h. Cozzolino et al. [50] investigated the influence of HTF temperature and flow rate in a tubes-in-tank unit. They found that when the HTF temperature increased from 80℃ to 90℃, the energy efficiencies were improved from 73.6% to 91.4% and 78.7% to 93.8% for the minimum and maximum flow rate, respectively. In other words, the HTF temperature, rather than the flow rate, has a more significant effect on the phase change process. In Martinelli et al. [59] ‘s research, the HTF injection sides were compared in a shell-and-tube unit. The total melting time was 500s and 810s for the top-injection HTF and the bottom-injection respectively, whereas the solidification time was 550s and 880s. It indicated that the top-injection configuration was more efficient for their experimental setup.

3. Numerical investigation on solid-liquid phase-change heat transfer in porous ss-PCM

Although experimental investigations can provide “directly interpretable” results of the phase change process, they are time-consuming and cannot depict some detailed flow and heat transfer characteristics, such as the flow field. Besides, it would be very expensive to experimentally investigate all the parameters influencing the phase change process of porous ss-PCMs [21, 64]. The numerical simulation provides an effective solution to address the problems and thus, a great number of researchers conducted numerical investigations [61].

Generally, the simulation methods for solid/liquid phase-change heat transfer in porous ss-PCMs can be classified into two categories: representative elementary volume (REV)-scale method and pore-scale method [65]. The schematic of the two

methods is presented in Fig. 9 and the comparison is listed in Table 6. The REV-scale simulation treats the porous ss-PCM as a uniformly mixed medium (see the typical computational domain in Fig. 10(a)) and does not require an accurate description of the support structure. In other words, it ignores the complex geometric information of the medium. Instead, this method utilizes some statistical parameters, such as porosity, permeability, and effective thermal conductivity, to characterize the porous structure. Therefore, it suits the simulation of porous media systems with large sizes. To account for the presence of a porous structure, terms based on semi-empirical models are added into the governing equation. Through choosing appropriate semi-empirical models, the REV-scale simulation can provide reasonable results. The REV-scale approach includes the traditional CFD methods, such as finite-difference method (FDM), finite-volume method (FVM) and finite-difference method (FDM), and the REV-scale lattice Boltzmann method.

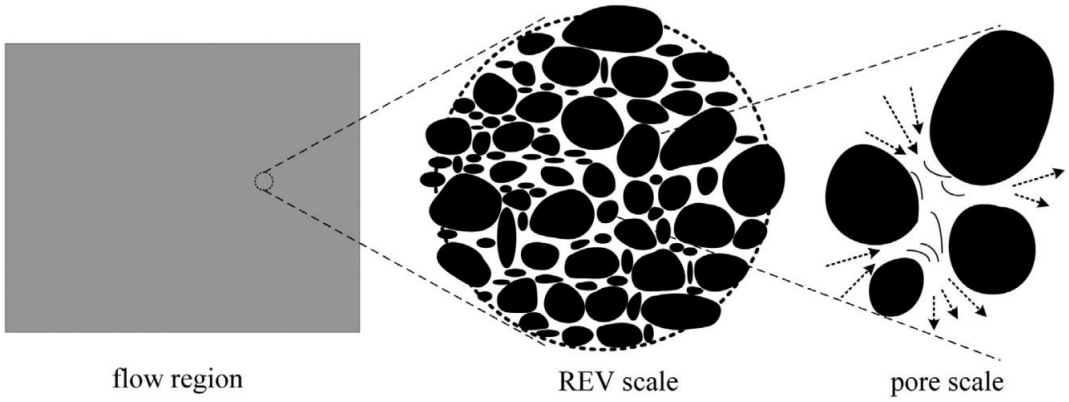

Fig. 9. Schematic of REV-scale and pore-scale method [66]

Table 6

Comparison between REV-scale and pore-scale simulation

Method	REV-scale simulation	Pore-scale simulation
Feature	Treat the porous ss-PCM as a uniform mixture commonly by volume average and simulate the phase change of the mixture	Directly simulate the phase change of PCM in porous structure
Advantages	(1) Simple input (2) Less computational sources required (3) Large simulated system	(1) Exhibiting flow and heat transfer in pores (2) Reflecting the effect of porous structure on phase change
Disadvantages	(1) Lack of flow and heat transfer characteristics in pores (2) Disability in revealing the effect of the porous structure	(1) High computational cost (2) Complex geometry input
Application conditions	Macroporous material	Macroporous material Mesoporous material Microporous material Hierarchical porous material
Simulation approach	FVM FEM FDM LBM	LBM DNS

The pore-scale method adopts the real porous microstructure of the support as the computational domain, as Fig. 10(b) shows. It directly models the interaction between PCM and the porous support. Therefore, it can reflect the influence of porous structure on the phase-change process and provide richer information than the REV-scale simulation. More importantly, since more and more microporous, mesoporous and hierarchical porous materials are employed as porous supports of ss-PCMs [11], the pore-scale simulation provides a remark inspiration for understanding the flow and heat transfer in pores of these new materials. As Lattice Boltzmann Method (LBM) possesses the robust ability to handle complicated boundaries, an increasing number of researchers employ LBM to perform the pore-scale simulation of phase-change heat transfer in porous ss-PCMs [67].

In this section, the REV-scale simulation by traditional CFD methods (e.g. FVM, FDM and FEM) will be introduced in section 3.1 while the pore-scale simulation based on the LB method in section 3.2.

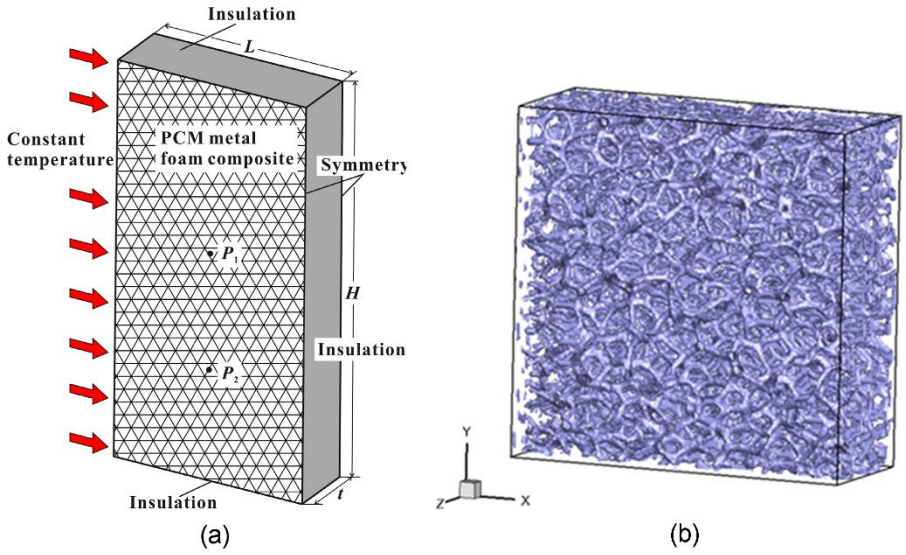

Fig.10 Typical computational domain in (a) REV-scale simulation [68] and (b) pore-scale simulation [69]

3.1 REV-scale simulation

According to the local thermal/non-thermal equilibrium, models used in the REV-scale method are classified into one-temperature model and two-temperature model [5]. The one-temperature model assumes there is a thermal equilibrium between PCM core and porous support. This model was first applied to investigate the melting of ice in the porous medium by Weaver et al. [28]. Due to its simple computation, several researchers continued to employ the one-temperature model to perform simulations on the phase-change heat transfer in porous ss-PCMs. The relating studies are listed in Table 7.

The one-temperature model is applicable when the thermal equilibrium between the PCM and porous supports can be achieved. However, since there is an apparent difference between the thermo-physical properties of the PCM core and support material, the macroscopic temperature of the two components is not always the same [70]. Hence, the one-temperature energy model is not valid in many cases.

Table 7

Summary of REV-scale simulation using one-temperature model

Ref	Material	Porosity	Dimensional
[36]	Paraffin/copper foam	0.95	2D
[34]	Paraffin/aluminum foam	0.77-0.95	2D
[71]	Docosane/aluminum foam	0.757-9898	2D
[72]	Docosane/ aluminum foam	0.97	2D
[73]	Paraffin/aluminum foam	0.75-0.94	3D
[74]	$NaNO_3$/copper foam	0.9	3D
[29]	Gallium/glass beads	0.385	2D
[28]	Water/Aluminium or galss beads	0.36-0.39	2D
[75]	Li_2CO_3 and Na_2CO_3/copper foam	0.95	2D

In contrast, the two-temperature model takes into account the temperature difference between the PCM and porous support, and thus it is more accuracy [9]. As a result, it is widely employed by researchers. This section will introduce the two-temperature model and its applications in simulating phase-change heat-transfer process of porous ss-PCMs.

3.1.1 Two-temperature model

3.1.1.1 Governing equations

Governing equations of the two-temperature model consist of continuity equation, momentum equations and two-temperature energy equations [5].

3.1.1.1.1 Continuity equation

Since the flow occurs in the liquid PCM region, the continuity equation is only established for the liquid PCM [9]:

$$\frac{\partial \rho_f}{\partial t} + \nabla \cdot \left(\rho_f \vec{U}\right) = 0 \tag{1}$$

If the flow is assumed incompressible, Eq. (1) reduces to:

$$\nabla \cdot \vec{U} = 0 \tag{2}$$

3.1.1.1.2 Momentum equation

To account for the existence of the porous support, a series of semi-empirical models are developed to model the flow in ss-PCMs, such as the Darcy model, the Forchheimer-extended Darcy model [76] and the Brinkman-extended Darcy model [77]. Taking into account the above models, the generalized non-Darcy momentum equations for liquid PCM are given by [5]

$$\frac{\rho_f}{\varepsilon}\frac{\partial u}{\partial t} + \frac{\rho_f}{\varepsilon^2}\left(\vec{U} \cdot \nabla u\right) = -\frac{\partial p}{\partial x} - \frac{\mu_f}{K}u - \frac{\rho_f F_l}{\sqrt{K}}|u|u + \frac{\mu_f}{\varepsilon}\nabla^2 u + A_s u \tag{3}$$

$$\frac{\rho_f}{\varepsilon}\frac{\partial v}{\partial t} + \frac{\rho_f}{\varepsilon^2}\left(\vec{U} \cdot \nabla v\right) = -\frac{\partial p}{\partial x} - \frac{\mu_f}{K}v - \frac{\rho_f F_l}{\sqrt{K}}|v|v + \frac{\mu_f}{\varepsilon}\nabla^2 v + A_s v \tag{4}$$

$$\frac{\rho_f}{\varepsilon}\frac{\partial w}{\partial t} + \frac{\rho_f}{\varepsilon^2}\left(\vec{U} \cdot \nabla w\right) = -\frac{\partial p}{\partial x} - \frac{\mu_f}{K}w - \frac{\rho_f F_l}{\sqrt{K}}|w|w + \frac{\mu_f}{\varepsilon}\nabla^2 w + \rho_f g\beta\left(T_f - T_{m1}\right) + A_s w \tag{5}$$

where u, v and w is velocity in x, y and z direction, respectively; the second term on the right side of above three equations accounts for the Darcy effect; the third term explains Forchheimer-extended Darcy effect; the fourth term represents the Brinkman-extended Darcy effect; the fifth term in Eq.(5), $\rho_f g\beta(T_f - T_{m1})$, denotes the natural convection driven by temperature difference; the last term is the superficial velocity source term to discriminate the solid-liquid region [78]. A_s is defined as

$$A_s = -A_{mushy}\frac{(1-f)^2}{f^3+\emptyset} \quad (6)$$

in which A_{mushy} is the mushy constant and commonly valued between 10^3 and 10^9 [79, 80]. $\emptyset$ is set to 0.01 in order to prevent the division by zero.

It is noteworthy that Eqs.(3) ~ (5) are comprehensive momentum equations. Some researchers simplified the equation group. For instance, Qu et al. [81] performed a 2D simulation on the solid-liquid phase change of paraffin/copper foam in a lithium ion battery. Only Eq.(3) and Eq.(5) were formulated to construct the momentum equation group. Zhu et al. [82] performed a simulation on the phase change process of PCM embedded in a finned metal foam, without considering the Forchheimer-extended Darcy effect. Liu et al. [83] simulated the melting process in a shell-and-tube TES system. They took into account the Forchheimer-extended Darcy effect by the term $-\frac{\rho_f F_l}{2}|u|u$, rather than $-\frac{\rho_f F_l}{\sqrt{K}}|u|u$ in Eq. (3).

3.1.1.1.3 Energy equation

In the two-temperature model, the energy equations for PCM and porous support are formulated separately.

For PCM [9, 78]:

$$\varepsilon\rho_f c_{pf}\frac{\partial T_f}{\partial t} + \varepsilon\rho_f c_{pf}\left(\vec{U}\cdot\nabla T_f\right) = (k_{fe}+k_{td})\nabla^2 T_f + h_{sf}a_{sf}\left(T_s - T_f\right) - \varepsilon\rho_f L\frac{df_l}{dt} \quad (7)$$

For porous skeleton:

$$(1-\varepsilon)\rho_s c_{ps}\frac{\partial T_s}{\partial t} = k_{se}\nabla^2 T_s - h_{sf}a_{sf}(T_s - T_f) \quad (8)$$

where k_{td} is thermal conductivity induced by dispersion; k_{fe} and k_{se} are the effective thermal conductivity of PCM and the solid support, respectively; h_{sf} is interfacial heat transfer coefficient; a_{sf} is interfacial surface area. The definitions of h_{sf} and a_{sf} can be found in [78]. The last term, $-\varepsilon\rho_f L\frac{df_l}{dt}$, in Eq. (7) acts as the source term to calculate the liquid fraction f_l. It denotes that the phase change is taken into account at each iteration. Readers could refer to Ref.[84] to find the detailed calculation method of f_l.

When the local thermal equilibrium is assumed, the two-temperature energy equations reduce to the one-temperature energy equation [83]:

$$\overline{\rho c}\frac{\partial T}{\partial t} + \rho_p c_p\left(\vec{U}\cdot\nabla T\right) = k_{eff}\nabla^2 T - \varepsilon\rho_p L\frac{df_l}{dt} \quad (9)$$

Where $\overline{\rho c}$ and k_{eff} are volume-averaged parameters and expressed as

$$\overline{\rho c} = (1-\varepsilon)\rho_s c_s + \varepsilon\rho_p c_p \quad (10)$$

$$k_{eff} = (1-\varepsilon)k_s + \varepsilon k_p \quad (11)$$

There are also some different forms of the two-temperature model. For example, in order to simulate the melting process in the paraffin/metal foam composite ss-PCM, Zhao et al. [30] proposed the following two-temperature energy equations:

$$(1-\varepsilon)\frac{\partial T_s}{\partial t} = k_{fe}\nabla^2 T_s - h_{sf}a_{sf}\frac{(T_s - T_f)}{d} \quad (12)$$

$$\varepsilon\frac{\partial T_f}{\partial t} = k_{se}\nabla^2 T_s + h_{sf}a_{sf}\frac{(T_s - T_f)}{d} \quad (13)$$

Compared with Eqs. (7) and (8), the effect of flow on the PCM temperature was not considered in Zhao et al. [30]'s model. Nithyanandam et al. [85] studied the heat transfer performance of a TES system enhanced by metal foam and heat pipe. In their numerical model, the influence of liquid flow on PCM temperature was also neglected.

Chen et al. [86] analyzed the heat transfer performance of a solar flat-plate collector with paraffin/metal foam ss-PCM. The energy equation for PCM was given by

$$\varepsilon\rho_f c_{pf}\frac{\partial T_f}{\partial t}+\rho_f c_{pf}\left(\vec{U}\cdot\nabla T_f\right)=\varepsilon k_P\nabla^2 T_f+h_v\left(T_s-T_f\right) \quad (14)$$

where h_v is the volumetric heat transfer coefficient; k_P is the thermal conductivity of PCM. In the above formulation, the effect of PCM thermal conductivity was characterized as εk_P, rather than $k_{fe}+k_{td}$ in Eq. (7). Hu et al. [71] employed the two-temperature model to simulate the phase change process in a micro-foam. In their model, the term $k_{fe}+k_{td}$ in Eq. (7) was replaced by k_{fe}.

3.1.1.2 Correlations of interfacial heat transfer coefficient

Effective thermal conductivity and interfacial heat transfer coefficient are two critical parameters for modelling phase change heat transfer in porous ss-PCMs. Some researchers have summarized correlations of effective thermal conductivity in their reviewer papers [5, 18]. Thus, in this section, we reviewed correlations of interfacial heat transfer coefficient used in numerical investigations on phase change heat transfer in porous ss-PCMs.

Interfacial heat transfer coefficient, h_{sf}, describes the thermal interaction between ligaments of the porous support and PCM. However, it is very difficult to measure the coefficient by experiments due to the complex support structure and complicated flow scenario in porous ss-PCMs. Therefore, most researchers used empirical correlations as a substitution. The commonly used correlations are listed in Table 8. Žukauskas [87]'s correlation was originally proposed in the study on heat transfer from tubes in crossflow and describes the forced flow around cylinders. To use this correlation in modelling phase change heat transfer in porous ss-PCMs, researchers treated the ligaments of porous support as smooth cylinders and assumed the laminar flow of

liquid PCM in porous support resembled the flow around cylinders. Žukauskas [87]'s correlation was employed by most researchers, such as Sardari et al. [88], Yang et al. [39], etc. Churchill et al. [89]'s correlation is another widely used expression to estimate the interfacial heat transfer coefficient. This correlation has been proved to achieve satisfactory results for the laminar flow from a horizontal cylinder. It is noted that this correlation fails to predict accurately in the case of $10^{-6} < Ra$ because some experimental values fall below the results by this correlation. Some researchers, such as Zhao et al. [90] and Srivatsa et al. [91], employed this correlation by treating the ligament of the porous support as cylinders based on structural characteristics. Kuwahara et al. [92] established a correlation for porous media from a set of numerical experiments. This correlation is based on a two-dimensional structure model of porous media and assumes a macroscopically uniform flow through a series of square rods. In this correlation, the effect of porosity is taken into account. The formula is adopted by some researchers to estimate h_{sf}, such as Chen et al. [86] and Zhu et al. [82]. Di Giorgio et al. [93] proposed a new method to directly calculate h_{sf} by using the Kelvin 3D model of the foam structure. They divided the melting process into three phases: solid-solid, melting and convective and thus three coefficients were determined. They found h_{sf} did not vary remarkably in the solid-solid and melting conditions and therefore they assumed h_{sf} was constant in the two phases. Later Caliano et al. [38] employed this approach in their numerical study on the cold thermal energy storage unit.

Table 8

Correlations of interfacial heat transfer coefficient

Correlations	Application conditions	Proposed by	Applied in
$h_{sf}=\begin{cases}0.76Re^{0.4}Pr^{0.37}k_f/d, 0<Re\le 40\\ 0.52Re^{0.5}Pr^{0.37}k_f/d, 40<Re\le 1000\\ 0.26Re^{0.6}Pr^{0.37}k_f/d, 1000<Re\le 20000\end{cases}$	Forced flow for cylinders in crossflow	Žukauskas [87]	[9, 20, 23, 35, 39, 68, 78, 81, 85, 94]
$h_{sf}=\frac{k_f}{d}\left(0.36+\frac{0.518{Ra_d}^{\frac{1}{4}}}{\left(1+\left(\frac{0.559}{Pr}\right)^{\frac{9}{16}}\right)^{\frac{4}{9}}}\right)$	Natural convection around a horizontal cylinder, $10^{-6}<Ra<10^{9}$	Churchill et al. [89]	[83, 90, 91, 95]
$h_{sf}=\frac{k_f}{d}\left(\left(1+\frac{4(1-\varepsilon)}{\varepsilon}\right)+0.5(1-\varepsilon)^{0.5}Re^{0.6}Pr^{\frac{1}{3}}\right)$	Porous media, $0.2<\varepsilon<0.9$	Kuwahara et al. [92]	[82, 86, 96]
$h_{sf}=\frac{1}{t_f}\int_0^{t_f}\left(\frac{\dot{q}_{par-foam}(t)\cdot a_c}{T(R,t)-\langle T\rangle_{PCM}(t)}dt\right)\left(\frac{1}{a_c}\right)$	PCM and metal foam	Di Giorgio et al. [93]	[38]

3.1.1.3 Model solution

Currently, there are three numerical methods employed to solve the nonlinear two-temperature model, such as FVM, FEM and FDM. A summary of REV-scale simulations using different numerical methods is given in Table 9. In addition, a statistics of numerical tools used in REV-scale simulation is presented in Fig. 11. The earliest numerical simulation was performed by Weaver and Viskanta in 1986. They utilized FDM to solve the model. Nevertheless, it is obvious from Fig. 11 that FVM is the most commonly used method. This may be attributed to the rapid development of commercial CFD software, such as Fluent because Fluent is based on FVM. As Fig. 11(b) shows, Fluent is widely used for simulation, promoting the application of FVM.

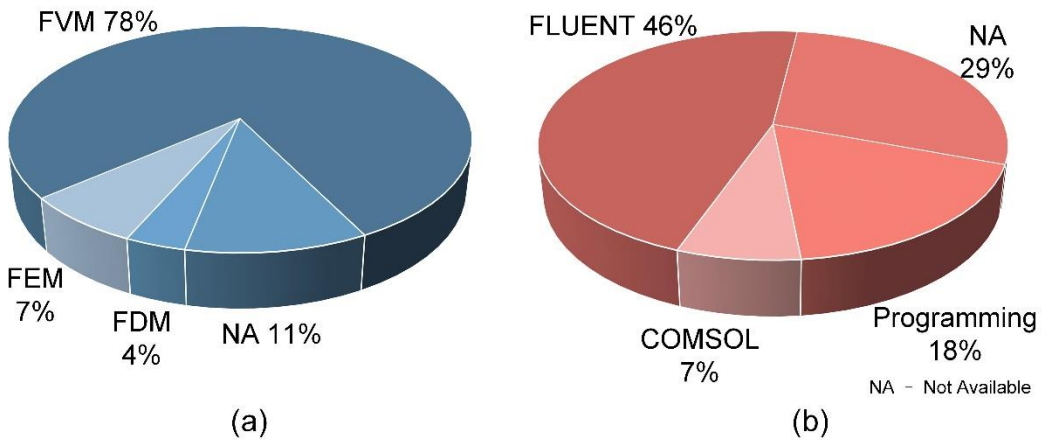

Fig. 11 Statistics of discrete methods (a) and numerical solution tools (b) employed in REV-scale simulation

Table 9

Summary of REV-scale simulation using two-temperature model

Ref	Material	Porosity	Pore size (mm)	Discrete method	Dimensional	Container
[37]	Paraffin/carbon-fiber brush	0.992-0.9932	-	-	3D	R
[97]	PCM/metal foam	0.385-0.8	1.92	FVM	2D	R
[30]	Paraffin/copper foam	0.95	2.54	FDM	2D	R
[86]	Paraffin/aluminum foam	0.90	-	FVM	2D	R
[98]	Paraffin/copper foam	0.85-0.95	0.85-2.54	FVM	2D	R
[9]	Paraffin/copper foam	0.90-0.98	0.635-2.54	FVM	2D	R
[81]	Paraffin/copper foam	0.90	1.27	FVM	2D	R
[91]	n-eicosane/ aluminum foam	0.86-0.94	0.85-2.54	FVM	2D	R
[99]	NaNO3/copper foam	0.855-0.945	0.635-1.27	FVM	2D	R
[71]	Docosane/aluminum foam	0.757-0.9898	0.36	-	3D	R
[96]	Paraffin/aluminum foam	0.90	1.25-5.08	FVM	2D	R
[20]	Paraffin/copper foam	0.97	1.016	FVM	3D	R
[82]	Sodium acetate/aluminum foam	0.865-0.965	1.27-5.08	FVM	2D	R
[35]	Paraffin/aluminum foam	0.859-0.958	-	FEM	3D	R
[68]	Paraffin/aluminum foam	0.90	5.08	FVM	2D/3D	R
[90]	Succinonitrile/copper foam	0.8-0.95	0.635-5.08	FVM	2D	R

[78]	Paraffin/copper foam	0.9-0.97	1	FVM	2D	R
[47]	eicosane/copper foam	0.95	0.125-2.54	-	2D	C
[100]	Paraffin /graphite foam	0.85-0.97	0.635-5.08	FVM	2D	C
[101]	Li_2CO_3 and K_2CO_3/copper foam Li_2CO_3 and K_2CO_3/SiC foam Li_2CO_3 and K_2CO_3/Al_2O_3 foam Li_2CO_3 and K_2CO_3/ nickel foam	0.95 0.95 0.95 0.95	1-5 4 4 4	FVM	2D	C
[83]	Paraffin/copper foam	0.95	0.42-2.54	FVM	2D/3D	C
[85]	Li_2CO_3 and Na_2CO_3/metal foam	0.85-0.95	0.635-2.54	FVM	3D	C
[23]	$NaNO_3$ and KNO_3/ metal foam	0.965-0.975	2.54	FVM	3D	C
[94]	Paraffin/ metal foam	0.94	1.69	FVM	2D	C
[39]	PCM/copper foam	0.93-0.97	0.85-3.18	FVM	2D	R
[88]	Paraffin/copper foam	0.85-0.95	0.51-2.54	FVM	3D	R
[95]	RT82/copper foam	0.95-0.98	0.64	FVM	2D	C
[38]	PCM/aluminum foam	0.935-0.955	2.54	FEM	2D	C

* C and R refer to cylindrical and rectangular, respectively.

3.1.2 Applications

A summary of REV-scale simulations based on the two-temperature model is given in Table 9. It covers literature from 2000 to 2019. Fig.12 gives the statistics of types of porous supports and pore size. It is found that most support materials are metal foam, and the pore size is over 0.1mm. In other words, all ss-PCMs studied are macroporous.

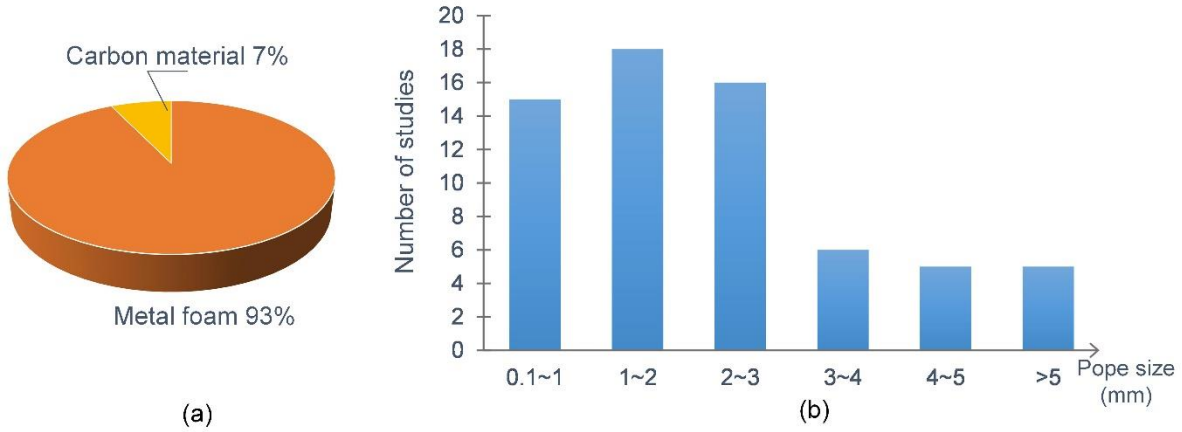

Fig. 12 Statistics of types of porous supports (a) and pore size (b) in REV-scale simulation

According to the difference in geometry, PCM containers are classified as rectangular and cylindrical ones [61]. The following two sections will introduce REV-scale simulations of porous ss-PCMs in rectangular and cylindrical container, respectively.

3.1.2.1 Rectangular container

A typical physical model of ss-PCM in rectangular container is shown in Fig. S2. In 2005, Krishnan et al. [97] investigated the melting process of PCM in a square container with the height of 142.2mm. They found that the metal foam acted in two aspects. On the one hand, it accelerated the heat response of PCM because of the high thermal conductivity; on the other hand, it dampened the natural convection due to the frictional resistance. In general, it improved the thermal response and lessened the overheating effectively. Later, Tian et al. [98] studied the phase change heat

transfer of paraffin/copper foam in a 200mm × 25mm rectangular container. Their results showed that metal foam significantly enhanced the heat conduction, and although it suppressed the convection, the metal foam improved the overall heat transfer performance of PCM. Srivatsa et al. [91] numerically investigated the phase change of ss-PCM enhanced by aluminium foam in a 80mm(length) x 62mm(width) x25mm(height) container. It was found that the natural convection was at the peak strength when PCM melted completely.

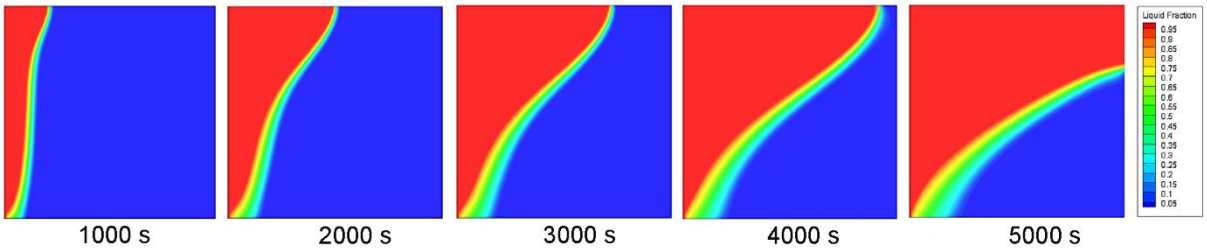

Fig. 13 Solid/liquid interface evolution of paraffin/copper foam composite ss-PCM simulated by Zhang et al. [20]

In 2017, Zhang et al. [20] demonstrated several stages where different heat transfer mechanisms dominated. As Fig. 13 shows, at the initial stage of 1000s, the melting interface was almost parallel to the left heating boundary, indicating that the conduction dominated the heat transfer. With time elapsed, more PCM melted and more high-temperature liquid PCM flowed upwards, pushing the upper solid/liquid interface moving. As a result, a sloped-shape interface was formed. At this stage, the natural convection was prominent in the phase change heat transfer. The simulation results were in good consistency with experimental observation shown in Fig. 5.

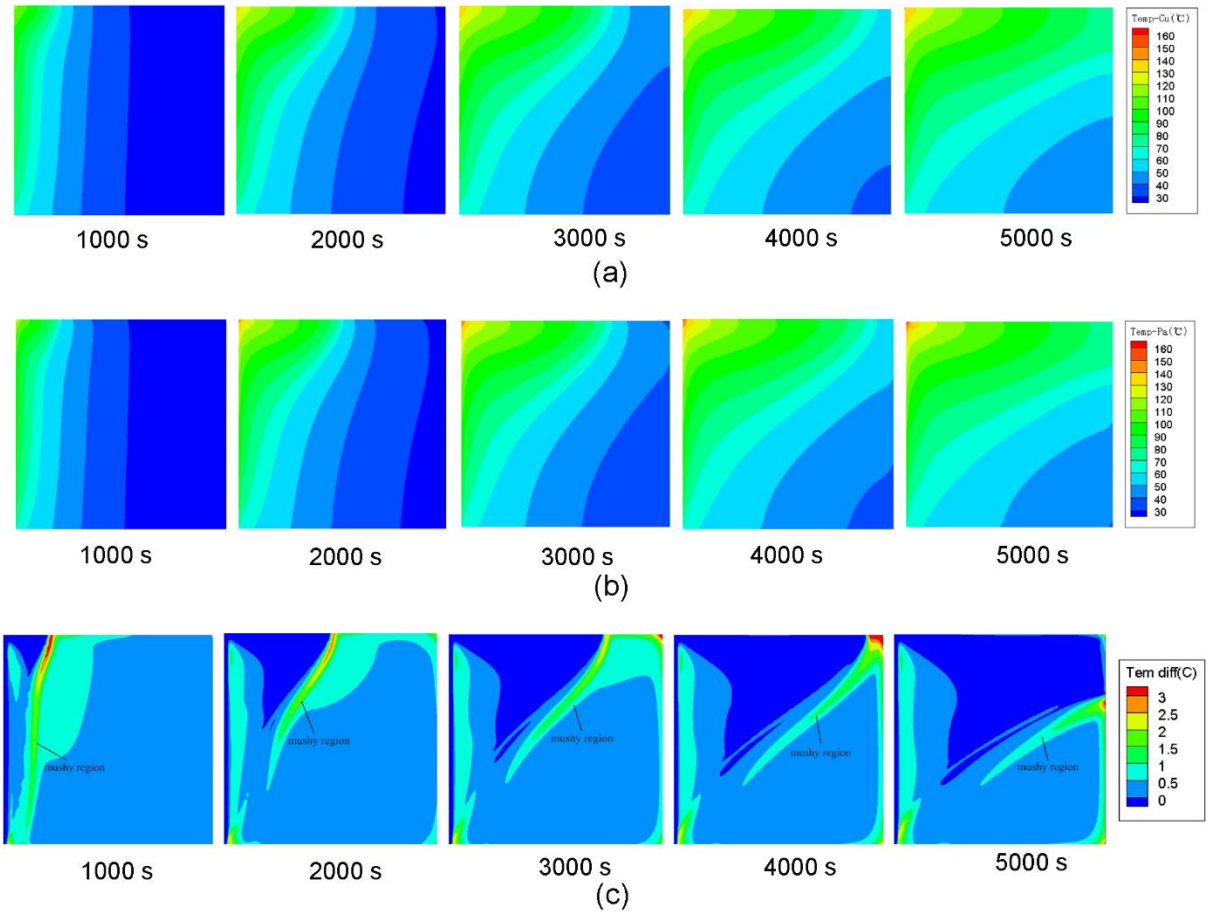

Fig. 14. Temperature field and temperature difference field of paraffin/copper foam porous ss-PCM simulated by Zhang et al. [20]: (a) copper foam; (b) paraffin; (c) temperature difference between copper foam and paraffin

Furthermore, in order to compare the temperature difference between PCM and porous support, Zhang et al. [20] simulated temperature fields of these two components, as shown in Fig. 14. The temperature of metal foam was generally higher than that of the PCM, especially in the PCM solid region where the heat conduction dominated the heat transfer. The temperature difference between the porous skeleton and PCM was large in the mushy region because the PCM was at the melting stage and the heat was absorbed as latent heat. After the PCM melted fully, natural convection occurred in the liquid region and enhanced the heat transfer, and thus, the temperature difference became very small. Li et al. [9] performed a numerical simulation on the melting process of porous ss-PCM in a 45mm x 100mm domain and

they found that in the same position, the temperature of porous support was higher than that of PCM. The researches above validated the feasibility and necessity of the two-temperature model.

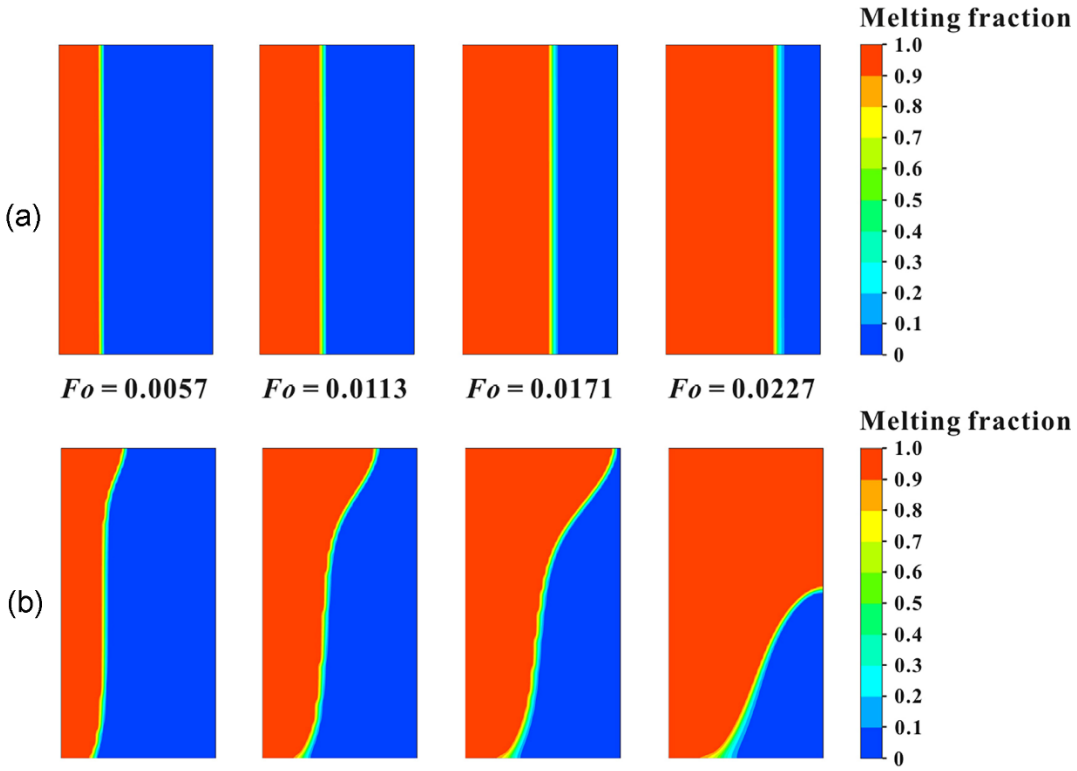

Fig. 15. Solid/liquid interface propagation (a) without considering natural convection (b) considering natural convection [68]

To compare effects of heat conduction and natural convection on the phase-change process, Yang et al. [68] conducted a simulation in a 76.2mm(length) × 152.4mm(height) × 25.4mm(width) domain. Their results are presented in Fig. 15. Without considering the natural convection, the melting front is parallel to the heated wall during the whole phase-change process because the liquid PCM is assumed to not flow. In contrast, taking into account the natural convection, a sloped-shape interface is formed. Yang et al. also compared contributions of the two heat transfer mechanisms to PCM melting and the results in Fig. S3 showed that, although the influence of natural convection was unignorable, heat conduction played a more

important role. From this point of view, it also explains the reason why the addition of high thermal-conductivity supports enhances the global heat transfer rate although it suppresses the natural convection.

Pore size and porosity of the porous support also exert effects on the phase-change heat-transfer performance of ss-PCM. In Tian et al. [98]'s study, metal foams with smaller porosity and pore size were recommended to improve the heat transfer rate because smaller pore size increased the contact area between PCM and the porous support and smaller porosity indicated more support materials embedded. Zhu et al. [96] investigated the thermal performance of paraffin/aluminum foam composite in a rectangular container and they found that using metal foam with smaller pore size could improve the thermal response of PCM. Zhao et al. [90] studied the solid-liquid phase-change heat transfer of succinonitrile/copper foam in a square container and analyzed the effect of porosity and pore size. The predicted results are shown in Fig. S4. As porosity decreased, the melting process was accelerated, while the difference in melting time tended to smaller. The phase change process could also be promoted by decreasing pore size because the larger interfacial area can be generated. The similar laws can be found in Sundarram et al. [73]'s study. Moreover, the laws are consistent with the experimental finding by Zhao et al. [30]. Yang et al. [99] numerically analysed the solid-liquid phase change of ss-PCM in a 10cm(width) x 30cm(height) domain. It was found that the heat transfer was enhanced and the total melting time was shorted by increasing porosity linearly from bottom to top, compared with that for a constant porosity, owing to the enhanced natural convection.

3.1.2.2 Cylindrical container

An example of physical model of ss-PCM in cylindrical container is shown in Fig. S5. In 2008, Lafdi et al. [100] numerically investigated the phase change process of

PCM/graphite foam in a cylindrical domain. They found that the heat transfer performance of the PCM system was enhanced significantly owing to the addition of high thermal-conductivity graphite foam. The average output power of the system enhanced by graphite foam was increased more than 8 times for the space application, while approximately 5 times for the terrestrial application. Liu et al. [83] performed a 3D simulation in a 40mm (inner diameter) x 82mm (inner diameter) x 250mm (length) computational domain. In their study, the solid/liquid interface propagation and temperature distribution etc. were predicted. As Fig. 16 shows, the temperature along the central tube decreased because the heat was absorbed by the surrounding PCM as the heat transfer fluid flowed. A 335K iso-surface moved from the inlet to the outlet during the melting process. The right side of the iso-surface was completely molten PCM while the left represented where the melting was proceeding. Later, Zhang et al. [23] studied the melting/solidification of ss-PCM in a vertical cylindrical storage unit. They used $NaNO_3$ and KNO_3 as PCM and found that the solid/liquid interface curved gradually during the melting process, indicating increasing natural convection; for the solidification process, the phase interface was almost parallel to the cooling wall, illustrating that the heat conduction was dominant.

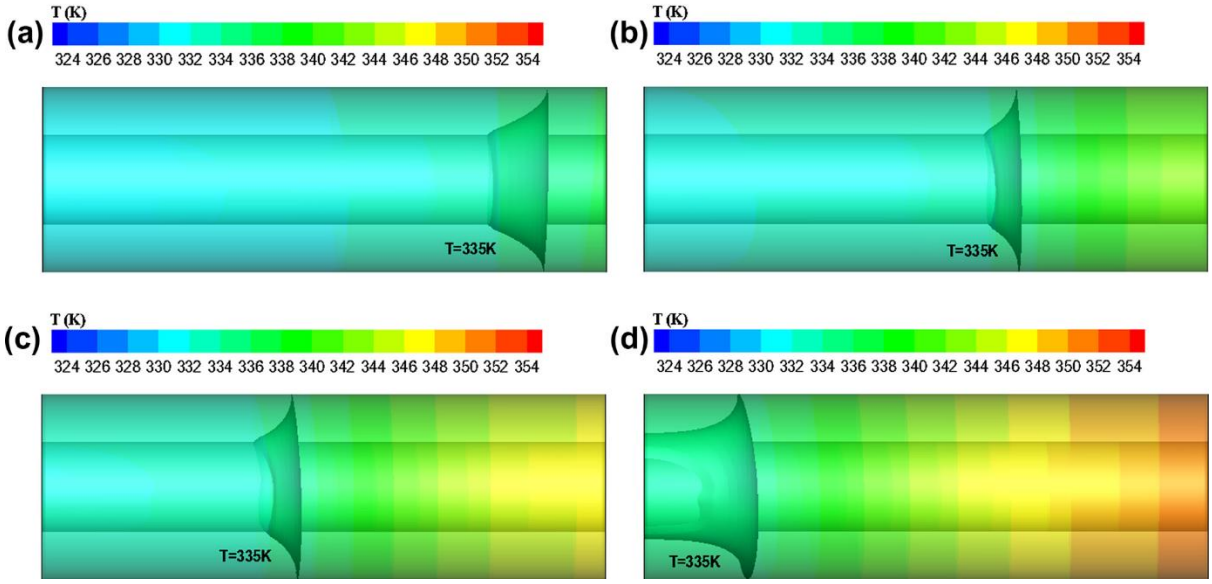

Fig. 16. Temperature field evolution during melting process in a cylindrical container [83]

Some researchers optimized the configuration of enhancers to improve thermal performance. For instance, Nithyanandam et al. [85] conducted a numerical study on the metal foam and heat pipe enhanced TES unit. They simulated the melting/solidification process of four different configurations: (1) no heat pipe; (2) no heat pipe-metal foam; (3) 2 horizontal heat pipes-metal foam; (4) 2 vertical heat pipes-metal foam. Among, the 2 vertical heat pipes with metal foam was recommended to improve melting/solidification efficiency. Later, Xu et al. [101] evaluated and optimized the melting performance of a cylindrical TES unit partially filled with a porous medium. The predicted temperature and flow field are presented in Fig. 17. Their research showed that, to make the most of natural convection and save cost, the porous medium should be placed in the lower part of the tube and the optimal filling height ratio was 0.7.

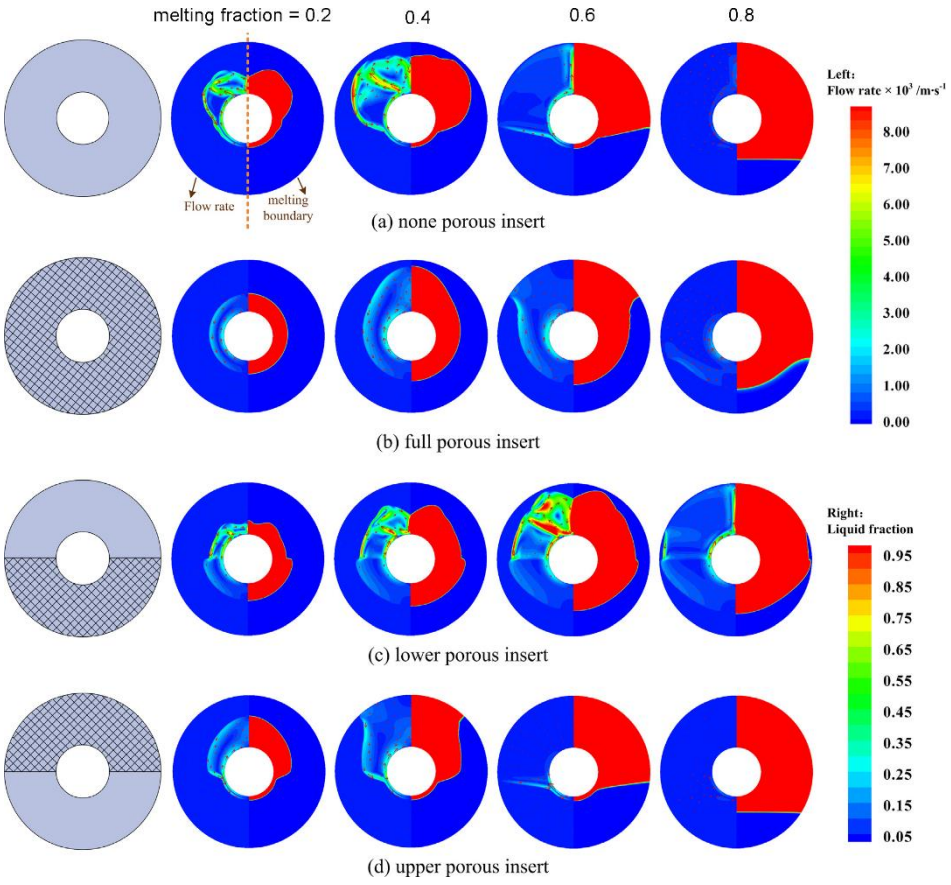

Fig. 17. velocity field (left semicircle) and melting interface (right semicircle) at different melting fractions [101]

3.2 Pore-scale LB simulation

The above simulations are continuum-based. Lattice Boltzmann method (LBM) is a relatively new approach which is particle-based and employs a simple kinetic model [102]. The principle of this numerical method is that, fluid is discretized into small particles and macroscopic heat and mass transfer characteristics are predicted by evolving thermal motion of fluid particles. Compared with the above numerical method, LB method has three advantages: (1) simple calculation procedure; (2) parallel computation; (3) robust ability to handle complex geometries [102, 103]. LBM was first proposed by McNamara et al. [104] for simulating fluid flow. Recently, many researchers employ it to investigate phase change phenomena in porous medium because it is inherently transient and thus suitable for investigating the transient phase change process [105]. LBM can perform the REV-scale simulation [106], however, its advantage of handling complex boundaries can be made the best by conducting the pore-scale simulation. This section will introduce the recent advancement of the pore-scale LBM simulation on the phase change heat transfer in porous ss-PCMs.

3.2.1 Pore-scale LB model

3.2.1.1 Governing equations

For the pore-scale simulation on the phase change heat transfer in porous ss-PCMs, the following assumptions are usually made [69, 107]:

(1) PCM and porous supports are homogeneous and isotropic;

(2) Liquid PCM is incompressible;

(3) Thermo-physical properties of PCM and porous supports are constant;

(4) Porous supports are rigid.

Based on the above assumptions, the continuity equation of PCM is simplified as [31]:

$$\nabla \cdot \boldsymbol{u} = 0 \tag{15}$$

Due to considering the real pore structure, the semi-empirical models are not needed, and the momentum equation can be expressed as:

$$\frac{\partial \boldsymbol{u}}{\partial t} + (\boldsymbol{u} \cdot \nabla)\boldsymbol{u} = -\frac{\nabla p}{\rho_f} + \nu_f \nabla^2 \boldsymbol{u} - \boldsymbol{g}\beta(T - T_{ref}) \tag{16}$$

The energy equation for the PCM is given by:

$$\frac{\partial(\rho_P H)}{\partial t} + \nabla \cdot \left(\rho_P C_P \boldsymbol{u} T_f\right) = \nabla \cdot (\lambda_P \nabla T) \tag{17}$$

For the porous support:

$$\frac{\partial(\rho_s C_s T)}{\partial t} = \nabla \cdot (\lambda_c \nabla T) \tag{18}$$

The total enthalpy *H* in Eq. (17) includes both sensible and latent enthalpy and is given by:

$$H = C_P T + f_l L \tag{19}$$

3.2.1.2 LB equation for velocity field

Macroscopic quantities i.e. velocity and temperature, are derived by calculating the hydrodynamic moments of distribution functions. These distribution functions are obtained from solving LB equations. According to the difference of collision term, LB equations are categorized into Bhatnagar-Gross-Krook (BGK) model and multiple relaxation time (MRT) model [66, 103].

3.2.1.2.1 BGK-LB model

In 2002, Guo et al. [108] proposed a comprehensive BGK-LB model to account for the effect of porous medium and the evolution equation was defined as:

$$f_i(\mathbf{x} + \mathbf{e_i}\Delta t, t + \Delta t) - f_i(\mathbf{x}, t) = -\frac{[f_i(x,t) - {f_i}^{eq}(x,t)]}{\tau_v} + \Delta t F_i \tag{20}$$

where f_i and ${f_i}^{eq}$ are the density distribution function and equilibrium density

distribution function, respectively. The equilibrium density distribution function f_i^{eq} is given by:

$$f_i^{eq} = \rho\omega_i \left[1 + \frac{\mathbf{e_i}\cdot\mathbf{u}}{{c_s}^2} + \frac{\mathbf{uu}:(\mathbf{e_i}\mathbf{e_i} - {c_s}^2\mathbf{I})}{2\varepsilon {c_s}^4}\right] \tag{21}$$

F_i is the forcing term and expressed as

$$F_i = \rho w_i (1 - \frac{1}{2\tau_v}) \left[\frac{\mathbf{e_i}\cdot\mathbf{F}}{{c_s}^2} + \frac{\mathbf{uF}:(\mathbf{e_i}\mathbf{e_i} - {c_s}^2\mathbf{I})}{\varepsilon {c_s}^4}\right] \tag{22}$$

in which $\mathbf{F}$ is the total body force:

$$\mathbf{F} = -\frac{\varepsilon\nu}{K}\mathbf{u} - \frac{\varepsilon F_\varepsilon}{\sqrt{K}}|\mathbf{u}|\mathbf{u} + \varepsilon\boldsymbol{g} \tag{23}$$

It should be noted that the total body force $\mathbf{F}$ includes the Darcy (the first term on the right hand) and Forchheimer drag force (the second term on the right hand). The evolution equation in Guo and Zhao's model can recover the macroscopic generalized non-Darcy equation through the Chapman-Enskog expansion [66].

However, for the pore-scale simulation, the semi-empirical correlations are not needed. Hence, many researchers simplified Guo and Zhao's BKG-LB model [109, 110]. Huo et al. [109] only considered the buoyancy force and defined $\mathbf{F}$ as:

$$\mathbf{F} = \rho\beta\boldsymbol{g}(T_{ref} - T) \tag{24}$$

This expression is also employed in Li et al. [110]'s model.

In addition, as the porosity ε is a statistic parameter for the REV-scale simulation, it is not needed in the pore-scale simulation. The equilibrium density distribution function f_i^{eq} and the forcing term F_i are rewritten as [109]

$$f_i^{eq} = \rho\omega_i \left[1 + \frac{\mathbf{e_i}\cdot\mathbf{u}}{{c_s}^2} + \frac{(\mathbf{e_i}\cdot\mathbf{u})^2}{2{c_s}^4} - \frac{u^2}{2{c_s}^2}\right] \tag{25}$$

$$F_i = \rho w_i (1 - \frac{1}{2\tau_v}) \left[\frac{\mathbf{e_i} - \mathbf{u}}{{c_s}^2} + \frac{\mathbf{e_i}\cdot\mathbf{u}}{{c_s}^4}\mathbf{e_i}\right]\boldsymbol{F} \tag{26}$$

Li et al. [69] utilized a more simplified form to define F_i:

$$F_i = \frac{w_i\rho\mathbf{e_i}}{{c_s}^2}\boldsymbol{F} \tag{27}$$

For the two dimensional (2D) cases, D2Q9 lattice scheme is commonly used for discretizing the velocity space [103] and the nine velocities in the D2Q9 lattice (Fig. S6) are expressed as:

$$\boldsymbol{e_i} = \begin{cases} (0,0) & i = 0 \\ c\left(\cos\left[\frac{(i-1)\pi}{2}\right], \sin\left[\frac{(i-1)\pi}{2}\right]\right) & i = 1,2,3,4 \\ \sqrt{2}c\left(\cos\left[\frac{(2i-1)\pi}{4}\right], \sin\left[\frac{(2i-1)\pi}{2}\right]\right) & i = 5,6,7,8 \end{cases} \quad (28)$$

Where i is the streaming direction, and c is the streaming speed defined as $c = \Delta x/\Delta t$, in which Δx and Δt are the lattice cell size and the lattice time step, respectively.

In contrast, D3Q6 [111], D3Q15 [111] and D3Q19 [69, 112] are usually employed for modelling the heat transfer in 3D geometries.

Finally, the macroscopic density and velocity are derived from [69]

$$\rho = \sum f_i \quad (29)$$

$$\rho \mathbf{u} = \sum \boldsymbol{e_i} f_i \quad (30)$$

3.2.1.2.2 MRT-LB model

The MRT-LB model was proposed by d'Humières et al. [113]. It has a different collision term from the BGK-LB model. The standard evolution equation of the MRT-LB model (without a forcing term) is expressed as [114, 115]:

$$f_i(\mathbf{x} + \mathbf{e_i}\Delta t, t + \Delta t) - f_i(\mathbf{x}, t) = -\mathbf{M}^{-1}\boldsymbol{\Lambda}[\mathbf{m}(\mathbf{x}, t) - \mathbf{m}^{eq}(\mathbf{x}, t)] \quad (31)$$

where $\mathbf{M}$ and $\boldsymbol{\Lambda}$ are the transition matrix and relaxation matrix, respectively. $\mathbf{m}$ and $\mathbf{m}^{eq}$ are the velocity moments of f_i and their equilibria:

$$\mathbf{m} = \left(\rho, e, \varepsilon, j_x - \frac{\Delta t}{2}\rho F_x, q_x, j_y - \frac{\Delta t}{2}\rho F_y, q_y, p_{xx}, p_{xy}\right)^T \quad (32)$$

$$\mathbf{m}^{eq} = \begin{pmatrix} \rho \\ -2\rho + 3\rho_0|\boldsymbol{u}|^2/\varphi \\ \rho - 3\rho_0|\boldsymbol{u}|^2/\varphi \\ \rho_0 u_x \\ -\rho_0 u_x \\ \rho_0 u_y \\ -\rho_0 u_y \\ \rho_0\left({u_x}^2 - {u_y}^2\right)/\varphi \\ \rho_0 u_x u_y/\varphi \end{pmatrix} \tag{33}$$

$\mathbf{M}$ linearly transforms the distribution function $\boldsymbol{f}$ into the velocity moment $\mathbf{m}$:

$$\mathbf{m} = \mathbf{M} \cdot \boldsymbol{f} \tag{34}$$

Although the MRT-LB model is widely applied in the REV-scale simulation [105, 115, 116], few studies employ the MRT-LB method to model the flow field in the pore-scale simulation.

3.2.1.3 LB equation for temperature field

3.2.1.3.1 Thermal BGK-LB model

The temperature field is derived from the thermal LB equation. The evolution equation of the thermal BGK-LB model without considering phase change can be expressed as [66]:

$$g_i(\mathbf{x} + \mathbf{e_i}\Delta t, t + \Delta t) - g_i(\mathbf{x}, t) = -\frac{[g_i(\mathbf{x},t) - {g_i}^{eq}(\mathbf{x},t)]}{\tau_g} \tag{35}$$

where g_i and ${g_i}^{eq}$ is the enthalpy distribution function and the equilibrium enthalpy distribution function:

$${g_i}^{eq} = \widetilde{\omega}_i \rho c_v T\left[1 + \frac{\mathbf{e_i}\cdot\mathbf{u}}{c_{sT}^2} + \vartheta\frac{\mathbf{uu}:(\mathbf{e_i}\mathbf{e_i} - c_{sT}^2\mathbf{I})}{2c_{sT}^2}\right] \tag{36}$$

in which $\widetilde{\omega}_i$ is the weight coefficients, c_{sT} is the sound speed of lattice, $\vartheta \in (0, 1)$.

For the porous support, due to the absence of flow, the equilibrium temperature distribution function is simplified as [109, 117]

$${g_i}^{eq} = \widetilde{\omega}_i \rho c_v T \tag{37}$$

Eq.(35) is the enthalpy -based thermal BGK-LB equation. Peng et al. [118], Shi

et al. [119] and Li et al. [120] simplified Eq.(35) into the temperature-based equation by assuming that the flow was incompressible and the thermal conductivity was constant. Correspondingly, g_i and ${g_i}^{eq}$represents the temperature distribution function and the equilibrium temperature distribution function:

$$ {g_i}^{eq} = \widetilde{\omega}_i T\left[1 + \frac{\mathbf{e_i}\cdot\mathbf{u}}{c_{sT}^2} + \vartheta\frac{\mathbf{uu}:(\mathbf{e_i}\mathbf{e_i} - c_{sT}^2\mathbf{I})}{2c_{sT}^2}\right] \tag{38} $$

τ_g is the relaxation time related to the thermal diffusivity coefficient α:

$$ \tau_g = \frac{\alpha}{c_{sT}^2\cdot\Delta t} + 0.5 \tag{39} $$

Considering the solid-liquid phase change, the enthalpy-based method distinguishes the solid phase and liquid phase through the liquid fraction. Due to its easy implementation, it is widely employed to simulate the solid-liquid phase change phenomena. The first enthalpy-based LB model for the solid-liquid phase change was proposed by Jiaung et al. [121]. They added a latent-heat source term S into the thermal BGK-LB equation and Eq.(35) was rewritten as

$$ g_i(\mathbf{x} + \mathbf{e_i}\Delta t, t + \Delta t) - g_i(\mathbf{x}, t) = -\frac{[g_i(\mathbf{x},t) - {g_i}^{eq}(\mathbf{x},t)]}{\tau_g} + \Delta t\widetilde{\omega}_i S \tag{40} $$

The source term S was defined as

$$ S = -\frac{L[f_l(\mathbf{x},t+\Delta t) - f_l(\mathbf{x},t)]}{c_p\cdot\Delta t} \tag{41} $$

Based on the Jiaung et al.'s model, Chatterjee et al. [122] introduced a thermodynamically consistent enthalpy updating scheme and guaranteed the convergence of the iteration process.

It is noteworthy that Jiaung et al. [121]'s and Chatterjee et al. [122]'s models are suitable for the conduction-dominated heat transfer. In 2008, Huber et al. [123] developed an LB model which incorporated the natural convection. They analyzed the transition from the conduction-dominated heat transfer to the fully developed convection. Their predicted results were in good consistency with scaling laws

calculated by Jany et al. [124].

Huber et al. [123]'s thermal BGK-LB model was utilized by Song et al. [125] to perform the pore-scale simulation of the freezing process in the soil. Chen et al. [31] employed Eq.(40) to simulate the melting process of paraffin/aluminum foam ss-PCM . The numerical results were in good agreement with experimental observations. Li et al. [69] used the thermal BGK-LB model to investigate the pore-scale heat-transfer performance in a 3D geometry. An interesting finding is that the secondary convection was captured in the transverse direction and neglecting the secondary convection in the 2D model led to a significant error in predicting heat transfer performance.

3.2.1.3.2 Thermal MRT-LB model

The thermal MRT-LB equation is given by [126]

$$g_i(\mathbf{x}+\mathbf{e_i}\Delta t, t+\Delta t) - g_i(\mathbf{x},t) = -(\mathbf{N}^{-1}\mathbf{Q}\mathbf{N})_{ij}(g_j - g_j^{eq})|_{(\mathbf{x},t)} \quad (42)$$

where $\mathbf{N}$ and $\mathbf{Q}$ is the transformation matrix and relaxation matrix, respectively.

The transformation matrix $\mathbf{N}$ relates the moment space $\mathbf{n}$ and the velocity space $\mathbf{g}$ [127]:

$$\mathbf{n} = \mathbf{N}\mathbf{g} \quad (43)$$

In the pore-scale simulation using thermal MRT-LB model, the D2Q9 lattice scheme is commonly employed [107, 128]. The transformation matrix $\mathbf{N}$ can be found in Ref. [129-131] while the relaxation matrix $\mathbf{Q}$ is expressed as

$$\mathbf{Q} = \mathrm{diag}(1, \xi_\alpha, \xi_\alpha, \xi_e, \xi_v, \xi_v, \xi_q, \xi_q, \xi_\varepsilon) \quad (44)$$

The equilibrium distribution function g_i^{eq} is given by Eq.(36) or Eq.(38). The equilibrium moment $\mathbf{n}^{eq}$ is given by

$$\mathbf{n}^{eq} = \mathbf{N}\mathbf{g}^{eq} \quad (45)$$

For the enthalpy-based MRT-LB model, the thermal conductivity k is expressed as

$$k = \rho c_v c_{sT}^2 (\tau_g - 0.5)\Delta t \tag{46}$$

while for the temperature-based MRT-LB model, the thermal diffusivity α is given by

$$\alpha = c_{sT}^2 (\tau_g - 0.5)\Delta t \tag{47}$$

The application of the thermal MRT-LB model in the pore-scale simulation is relatively less compared with that of the thermal BGK-LB model. Ren et al. [128] employed the thermal MRT-LB model to perform the pore-scale simulation of the melting process in a metal foam. One year later, they utilized this model for another time to numerically investigate the phase-change process in a heat pipe-assisted metal foam.

3.2.2 Applications

3.2.2.1 Reconstruction of porous structure

To perform the pore-structure simulation, the first step is describing the pore structure of the ss-PCM. Currently, there are four methods to reconstruct the pore structure: (1) X-ray computed tomography (CT) [132, 133] (2) quartet structure generation set (QSGS) method [134, 135] (3) hard-sphere Monte-Carlo method [136] (4) random obstacle location method [137]. The comparison of these methods is presented in Table S1.

Among the four approaches, X-ray CT and QSGS methods are commonly utilized to construct the computational domain in simulating the phase-change heat-transfer process of porous ss-PCMs. For instance, Ren et al. [128] employed the QSGS method to reconstruct the microstructure of 20mm × 20mm metal foam (Fig. 18). The pore size ranged from 0.5mm to 1.0mm. One year later, they utilized this approach for another time to construct the porous structure of a heat pipe-assisted TES unit [107]. In contrast, Liu et al. [111] employed the X-ray CT approach and reconstructed a 5mm × 5mm × 5mm geometry. Li et al. [110] used X-ray CT to obtain the detailed geometric information of the ss-PCM structure. As a great number of computational resources would be consumed if the entire reconstructed domain was considered, they extracted a 20mm × 20mm computational domain to perform the simulation , as shown in Fig. 18(b1) and (b2). Other applications of methods of reconstructing ss-PCM structure are list in Table 10.

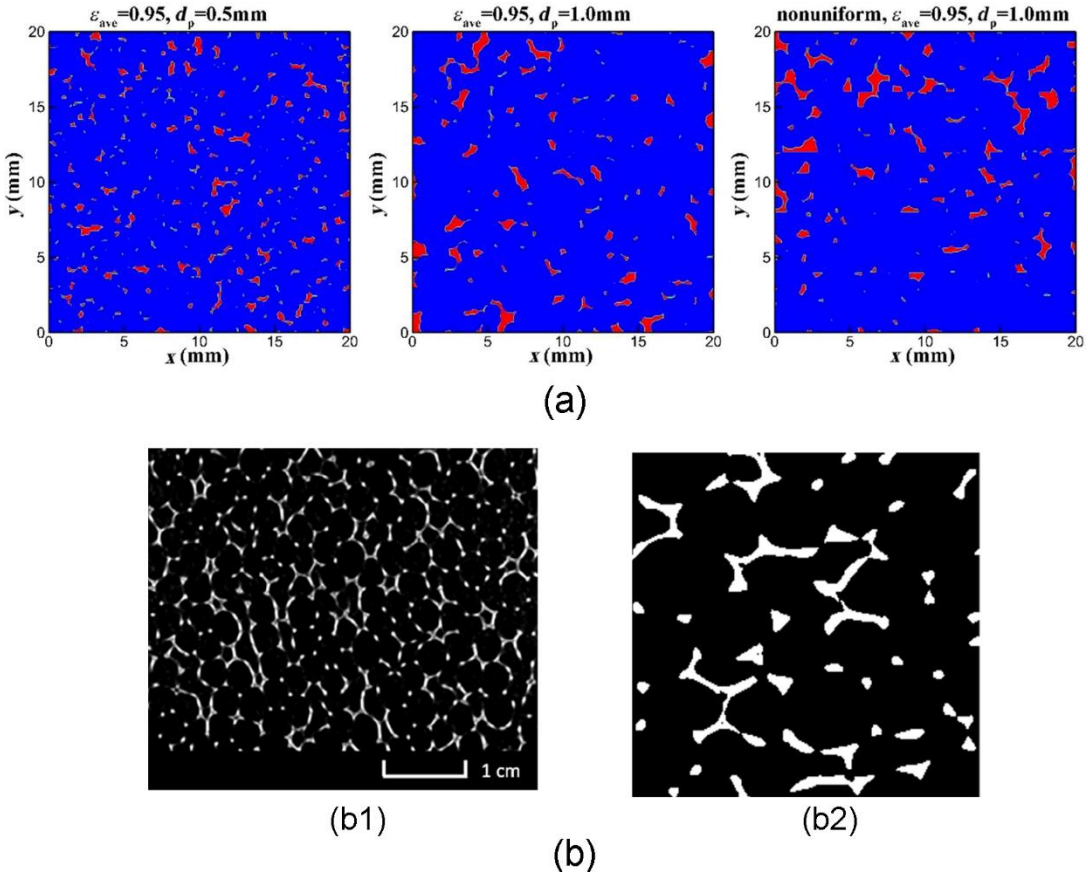

Fig. 18. Reconstructing 2D porous structure of ss-PCM using different methods (a) QSGS method [128] (b) X-ray CT: (b1) the entire reconstructed domian (b2) extracted domian for simulation [110]

Table 10

Summary of pore-scale LB simulation on phase change heat transfer in porous ss-PCMs

Ref	LB model for velocity field	LB model for temperature field	Porosity	Pore size (mm)	Type of porous medium	Discrete velocity model	Boundary scheme
[110]	BGK	Thermal BGK	0.9-0.94	-	Metal foam	D2Q9	Bounce back
[69]	BGK	Thermal BGK	0.88	-	Metal foam	D3Q19	Bounce back
	BGK	Thermal BGK	0.88	-	Metal foam	D2Q9	Bounce back
[117]	BGK	Thermal BGK	0.9	-	Metal foam	D2Q9	Bounce back
[107]	BGK	Thermal MRT	0.95	0.75	Metal foam	D2Q9	Immersed boundary scheme
[31]	BGK	Thermal BGK	0.9137	2.82	Metal foam	D2Q9	non-equilibrium extrapolation scheme
[128]	BGK	Thermal MRT	0.9-0.98	0.5-1.25	Metal foam	D2Q9	Bounce back
[109]	BGK	Thermal BGK	0.6-0.9	-	Metal foam	D2Q9	-
[125]	BGK	Thermal BGK	0.40-0.55	-	Soil	D2Q9	Bounce back

3.3.2.2 Comparison of simulation results by pore- and REV-scale method

3.3.2.2.1 Temperature field and phase interface

In 2018, Li et al. [110] studied the solid-liquid phase-change process in the metal foam at the pore scale. The structure-performance relation of PCM was analyzed under different gravity circumstances. The predicted results agreed well with the previous analytical and numerical results. In their study, the computational domain was heated by the left wall. To compare the results between the pore- and REV-scale simulation, we select Zhang et al. [20]'s investigation whose physical model was also heated by the left wall. As Fig. 19 shows, the overall distribution of the temperature field predicted by pore- and REV-scale method is similar: at the initial stage, the temperature contours were approximately parallel to the heating wall. With the elapse of time, more PCM melted and the effect of the natural convection was increasingly significant, leading to slope-shape isotherms.

Compared to the REV-scale simulation, the pore-scale simulation can reflect the influence of the porous structure. As seen from Fig. 19, the isotherms predicted by the pore-scale method were not as smooth as those by the REV-scale method. In the pore-scale simulation, some parts of the isotherms were parallel to the skeleton interface (see the marked area in Fig. 19(a)), indicating that the porous structure exerted an effect on the temperature distribution. However, this phenomenon cannot be simulated by the REV-scale method. In fact, the pore-scale simulation result is more reasonable. The pore distribution is ununiform, and some support protrudes at the interface; due to the high thermal conductivity, the support temperature is higher, leading to the melting of PCMs surrounding the support and forming an irregular interface.

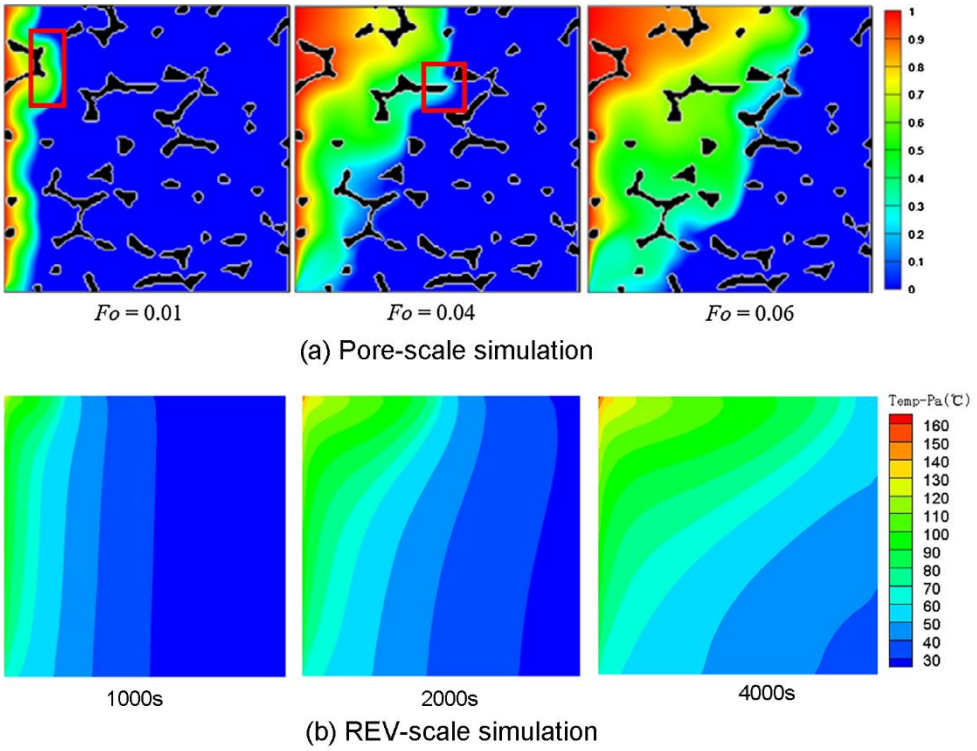

Fig. 19. Comparison of temperature fields predicted by different scale methods [20, 110]

The temperature evolution leads to the occurrence of solid/liquid phase change. The effect of pore structure is presented more clearly through the comparison of solid/liquid interfaces in Fig. 20. As this figure shows, in the pore-scale simulation, the phase interface is zig-zag-shaped and many parts of the interface are parallel to the skeleton, while in REV-scale simulation, this detailed information cannot be captured.

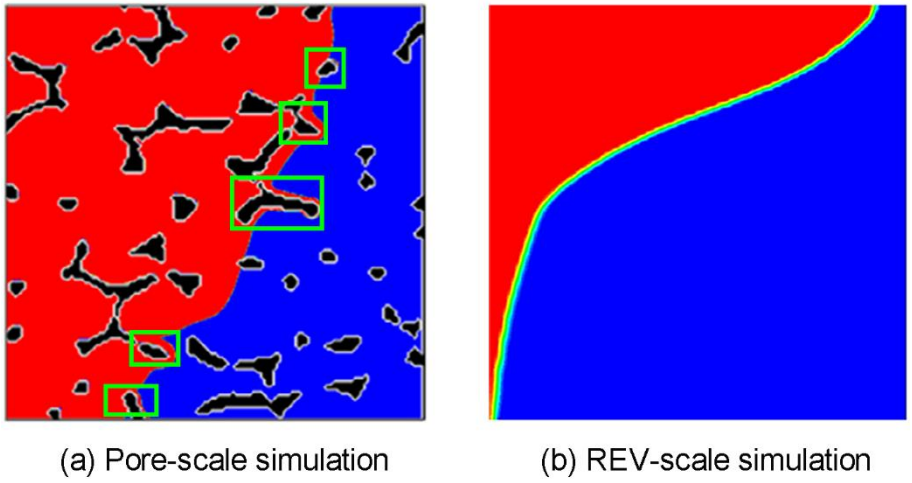

Fig. 20. Comparison of solid/liquid interfaces predicted by different scale methods [110] [20]

Ren et al. [128] simulated the melting process in a 20mm × 20mm square tank.

They found that PCM close to the skeleton melted faster than that far away. Huo et al. [109] investigated the melting process in a paraffin/aluminum porous ss-PCM with various porosities. They generated the porous structure via QSGS method. As more porous medium was located in the right region, PCM at this area melted more quickly. The above pore-scale investigations illustrate that the phase change heat transfer in porous ss-PCMs is affected by the porous structure, while the REV-scale simulation neglect the influence of the porous structure.

3.3.2.2.2 Flow field

Ren et al. [128] simulated the flow field of the phase change process as shown in Fig. 21(a). It can be clearly seen that the flow of liquid PCM was driven by the buoyancy force and passed through the gap between the support. At $Fo = 0.06$, the natural convection was further developed and a large vortex was formed in the middle field. The typical flow field simulated by the REV-scale method [68] is also presented in Fig. 21(b). It can be observed that the detailed flow through pores was ignored and the flow field was simplified greatly. Later, Ren et al. [107] studied the melting process of nanoparticle-PCM in a heat pipe-assisted TES unit. They found that the liquid PCM flowed through the gap between the metal foam and formed a small vortex at the early stage while the vortex did not occur in the case of high porosity and nanoparticle volume fraction.

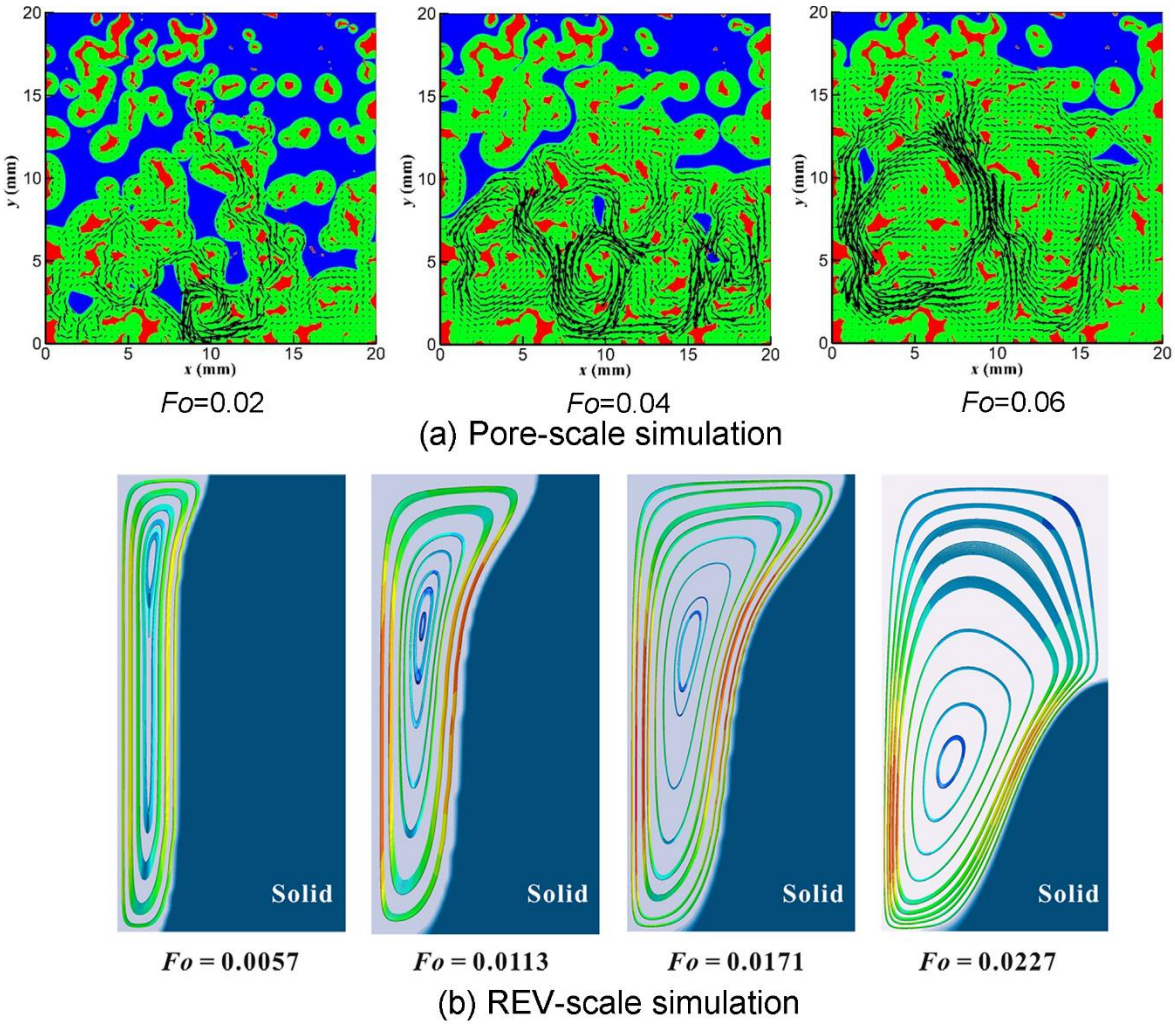

Fig. 21. Comparison of flow fields predicted by different scale methods: red, green, blue and black arrow in (a) represent skeleton, melted PCM, solid PCM and velocity vector, respectively [128] [68]

In Li et al. [110]'s pore-scale simulation, a large vortex was formed with a clockwise direction while some small vortices were generated due to the shear stress. At the top area, the circulation drove the high-temperature PCM to the low-temperature region while at the bottom area, it dragged the low-temperature PCM to the high-temperature region. The detailed description of the flow field can also be found in Huo et al. [109]'s investigation. The flow patterns are shown in Fig. 22. The flow was weakened in the nearly closed pores while it was accelerated in the pore throats.

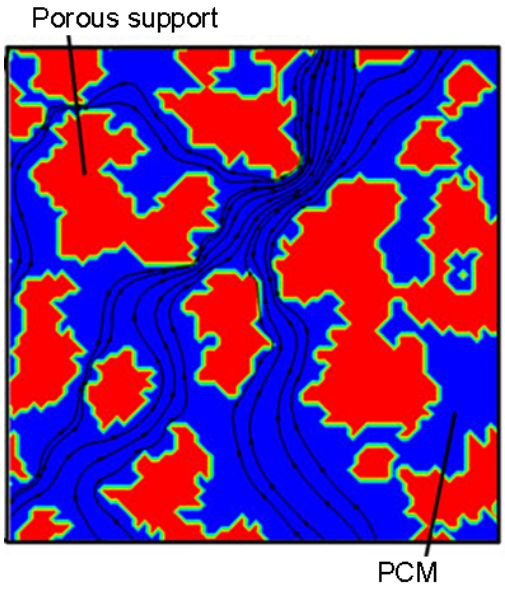

Fig. 22. Streamlines in pores simulated by the pore-scale method [109]

In summary, the pore-scale simulation can provide the overall phase-change heat-transfer characteristics like the REV-scale simulation. More importantly, it is able to display the flow and heat transfer in pores. This advantage is of great importance especially for mesoporous, microporous and hierarchical porous materials because the pore effect is significant in these supports [11, 12]. In other words, when investigating phase change heat transfer in these support materials, the support structure must be considered. Hence, the pore-scale simulation enables researchers to investigate the influence of pores on the phase change heat transfer in porous ss-PCMs and this method should be paid much more attention.

Both experimental and numerical studies on phase change heat transfer in porous ss-PCMs are counted and the results are shown in Fig. 23(a). We also count investigations on support material preparations for LHTES in the recent 20 years and the outcomes are presented in Fig. 23(b) and (c). It is found that all the studies on phase change heat transfer are performed on macroporous ss-PCMs while investigations on mesoporous, microporous and hierarchical porous ss-PCM are lacking. Furthermore, although the preparation of macroporous support materials

dominated in the early 15 years, nanoporous materials, especially mesoporous and hierarchical porous materials, develop rapidly in recent years. In other woods, there exists a research gap between material preparation and phase change heat transfer. To make the best of new materials, more efforts should be devoted to investigating phase change heat transfer in mesoporous, microporous and hierarchical porous ss-PCMs.

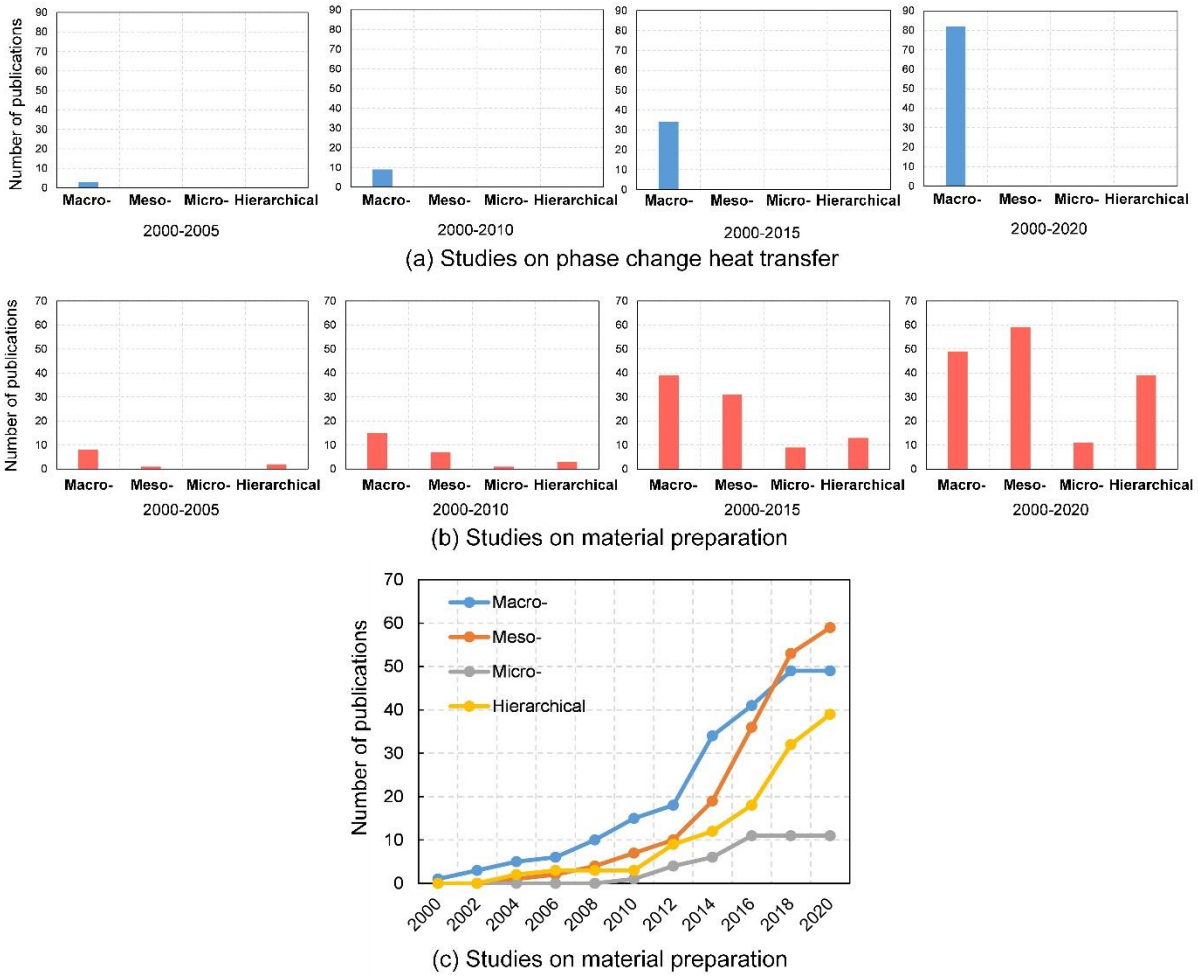

Fig. 23. Statistics of studies on porous ss-PCMs: (a) number of publications of phase change heat transfer in the recent 20 years (b) number of publications of material preparation for LHTES (c) trend of studies on material preparation (macro-, meso-, micro-, hierarchical represent macroporous, mesoporous, microporous and hierarchical porous, respectively)

4. Conclusion and outlook

Latent thermal energy storage continues to play an important role in solving the

mismatch between energy supply and demand. Shape-stabilized phase change materials based on porous supports have emerged as novel materials to address problems of PCM leakage and low thermal conductivity. This review summarizes the recent advances in experimental and numerical researches on the phase change heat transfer in porous ss-PCMs and provides a better understanding of the thermal-fluidic performance of composite materials. Materials, methods, apparatuses and significant results are involved in the section of experimental studies. Paraffin and metal foams are the most used PCM and porous support respectively in the reviewed experiments. Two simulation methods, i.e. REV-scale method and pore-scale method, are compared and it is concluded that the pore-scale simulation can provided the extra flow and heat transfer characteristics in pores. Although some significant progress has been made in investigating phase change heat transfer in porous ss-PCMs, great efforts are still required in future researches, including the following highlights:

(1) The coverage of PCMs used in current studies is very narrow. As Fig. 2 shows, the phase change temperature of overwhelming PCMs is from 0℃ to 70℃, within the range of low-temperature PCMs. For the middle/high-temperature LHTES applications, such as industrial waste heat recovery, researchers should broaden the selection of PCMs with higher phase change temperature.

(2) There exists a research gap between phase change heat transfer and material preparation. Both experimental and numerical investigations focus on macroporous ss-PCMs. However, the preparation of nanoporous materials, especially mesoporous and hierarchical porous materials, for LHTES has developed rapidly in recent years. In order to make the best of new materials, it is essential to investigate the phase change heat transfer in mesoporous, microporous and hierarchical porous ss-PCMs in the future.

(3) The pore-scale method exhibits great potential for the simulation of mesoporous, microporous and hierarchical porous materials and LBM is a suitable simulation tool due to its transient inherence. However, according to previous researches, the thermodynamic properties of PCMs in nanoporous supports changes a lot due to the size effect and confinement effect. Thus, to explore the phase change heat transfer in nanoporous ss-PCMs, researchers may adopt LBM with other advanced methods, such as molecular dynamics simulation.

Conflicts of interest

There are no conflicts to declare.

Acknowledgments

The authors acknowledge the financial support for this work from China National Key Research and Development Plan Project (No. 2018YFA0702300), National Natural Science Foundation of China (Grant No. 51676060), European H2020-MSCA-RISE (778104) of ThermaSMART project, Jilin Province Science and Technology Development Plan Project (No. 20180414021GH), the doctoral degree scholarship of China Scholarship Council (CSC), and Royal Academy of Engineering under Newton Fund - the UK-China Industry Academia Partnership scheme (UK-CIAPP\201).

Nomenclature

PCM	Phase change material
TES	Thermal energy storage
LHTES	Latent heat thermal energy storage

CFD	Computational fluid mechanics
LBM	Lattice Boltzmann method
PPI	Pores per inch
VAM	Volume-averaged method
DNS	Direct numerical simulation
SIMPLE	Semi-Implicit Method for Pressure Linked Equations
FVM	Finite volume method
FDM	Finite difference method
FEM	Finite element method
HD	High definition
DDF	Double distribution function
TDF	Triple distribution function
LTE	Local thermal equilibrium
LTNE	Local thermal non-equilibrium
REV	Representative Elementary Volume
MRT	Multi-relaxation time
BGK	Bhatnagar-Gross-Krook
TLBM	Enthalpy-based lattice Boltzmann model with basic evolution variable of temperature T
HLBM	Enthalpy-based lattice Boltzmann model with basic evolution variable of enthalpy H
QSGS	Quartet structure generation set
EB	Enthalpy based
TB	Temperature based
CT	Computed tomography

HTF	Heat transfer fluid
MOF	Metal-organic framework
PCP	Porous coordination polymer
HPP	Hierarchical porous polymer
HPC	Hierarchical porous carbon
CNT	Carbon nanotube
t	Time
u, v	Velocity in x and y directions
f_l	Liquid fraction in the pore
P	Pressure
x, y	Cartesian coordinates
Fo	Fourier number
l, h, w	Length, height, width
μ	Dynamic viscosity
K	Permeability
C_I	Inertial coefficient
A	Additional term in the momentum equation
g	Gravitational acceleration
T	Temperature
T_{m1}	The lower limit of melting point
c_{pf}	Specific heat capacity of PCM
c_{ps}	Specific heat capacity of porous support
k_{se}	Effective thermal conductivity of porous support
h_{sf}	Interfacial heat transfer coefficient

a_{sf}	Interfacial surface area
d_{ou}, od	Outer diameter
d_{in}, id	Inner diameter
$\vec{U}, \boldsymbol{u}$	Velocity vector
$\boldsymbol{F}$	Total body force per unit mass
F_{ε}	Forchheimer form coefficient
q	Internal heat production per unit volume
d_p	Pore diameter
H	Enthalpy
L	Latent heat
k	Thermal conductivity
Re	Reynolds number
Pr	Prandtl number
Ra	Rayleigh number
$\langle T \rangle_{PCM}$	Paraffin cell medium temperature
$\dot{q}_{par-foam}$	Heat flux on the whole paraffin surface
$T(R,t)$	Imposed boundary condition
a_c	Fraction of the cell external area

Greek letters

ε	Porosity
ω	Pore density
ρ	Density
δ	Liquid fraction ($= \varepsilon f_l$)
β	Thermal expansion coefficient

ν	Kinematic viscosity
α	Thermal diffusivity coefficient

Subscripts

f	Fluid (both solid and liquid)
fl	Liquid paraffin
tb	Thermal dispersion
s	Solid support
e	Effective or equivalent
ave	Average
p	PCM
c	Low
h	High
ref	Reference

References

[1] International Energy Agency (IEA). World Energy Outlook 2018, https://webstore.iea.org/world-energy-outlook-2018; 2019, [accessed 2019].

[2] Zhang H, Baeyens J, Caceres G, Degreve J, Lv Y. Thermal energy storage: Recent developments and practical aspects. Prog Energy Combust Sci. 2016;53:1-40.

[3] Kuravi S, Trahan J, Goswami DY, Rahman MM, Stefanakos EK. Thermal energy storage technologies and systems for concentrating solar power plants. Prog Energy Combust Sci. 2013;39:285-319.

[4] Pielichowska K, Pielichowski K. Phase change materials for thermal energy storage.

Prog Mater Sci. 2014;65:67-123.

[5] Zhang P, Xiao X, Ma ZW. A review of the composite phase change materials: Fabrication, characterization, mathematical modeling and application to performance enhancement. Appl Energy. 2016;165:472-510.

[6] Cabeza LF. Advances in thermal energy storage systems: Methods and applications. Cambridge: Woodhead Publishing; 2015.

[7] Sharma A, Tyagi VV, Chen CR, Buddhi D. Review on thermal energy storage with phase change materials and applications. Renew Sustain Energy Rev. 2009;13:318-45.

[8] Huang X, Chen X, Li A, Atinafu D, Gao H, Dong W, Wang G. Shape-stabilized phase change materials based on porous supports for thermal energy storage applications. Chem Eng J. 2019;356:641-61.

[9] Li WQ, Qu ZG, He YL, Tao WQ. Experimental and numerical studies on melting phase change heat transfer in open-cell metallic foams filled with paraffin. Appl Therm Eng. 2012;37:1-9.

[10] Fang G, Tang F, Cao L. Preparation, thermal properties and applications of shape-stabilized thermal energy storage materials. Renew Sustain Energy Rev. 2014;40:237-59.

[11] Feng D, Feng Y, Qiu L, Li P, Zang Y, Zou H, Yu Z, et al. Review on nanoporous composite phase change materials: Fabrication, characterization, enhancement and molecular simulation. Renew Sustain Energy Rev. 2019;109:578-605

[12] Gao H, Wang J, Chen X, Wang G, Huang X, Li A, Dong W. Nanoconfinement effects on thermal properties of nanoporous shape-stabilized composite PCMs: a review. Nano Energy. 2018;53:769-97.

[13] Umair MM, Zhang Y, Iqbal K, Zhang S, Tang B. Novel strategies and supporting

materials applied to shape-stabilize organic phase change materials for thermal energy storage–A review. Appl Energy. 2019;235:846-73.

[14] Li A, Wang J, Dong C, Dong W, Atinafu DG, Chen X, Gao H, et al. Core-sheath structural carbon materials for integrated enhancement of thermal conductivity and capacity. Appl Energy. 2018;217:369-76.

[15] Uemura T, Yanai N, Watanabe S, Tanaka H, Numaguchi R, Miyahara MT, Ohta Y, et al. Unveiling thermal transitions of polymers in subnanometre pores. Nat Commun. 2010;1:83.

[16] Tang J, Yang M, Yu F, Chen X, Tan L, Wang G. 1-Octadecanol@ hierarchical porous polymer composite as a novel shape-stability phase change material for latent heat thermal energy storage. Appl Energy. 2017;187:514-22.

[17] Zhang X, Lin Q, Luo H, Luo S. Three-dimensional graphitic hierarchical porous carbon/stearic acid composite as shape-stabilized phase change material for thermal energy storage. Appl Energy. 2020;260:114278.

[18] Rehman T-u, Ali HM, Janjua MM, Sajjad U, Yan W-M. A critical review on heat transfer augmentation of phase change materials embedded with porous materials/foams. Int J Heat Mass Transfer. 2019;135:649-73.

[19] Kenisarin MM, Kenisarina KM. Form-stable phase change materials for thermal energy storage. Renew Sustain Energy Rev. 2012;16:1999-2040.

[20] Zhang P, Meng ZN, Zhu H, Wang YL, Peng SP. Melting heat transfer characteristics of a composite phase change material fabricated by paraffin and metal foam. Appl Energy. 2017;185:1971-83.

[21] De Schampheleire S, De Jaeger P, De Kerpel K, Ameel B, Huisseune H, De Paepe M. How to study thermal applications of open-cell metal foam: Experiments and computational fluid dynamics. Materials. 2016;9:94.

[22] Weaver JA, Viskanta R. Freezing of water saturated porous media in a rectangular cavity. Int Commun Heat Mass. 1986;13:245-52.

[23] Zhang P, Xiao X, Meng ZN, Li M. Heat transfer characteristics of a molten-salt thermal energy storage unit with and without heat transfer enhancement. Appl Energy. 2015;137:758-72.

[24] Righetti G, Lazzarin R, Noro M, Mancin S. Phase change materials embedded in porous matrices for hybrid thermal energy storages: Experimental results and modeling. Int J Refrig. 2019;106:266-77.

[25] Mallow A, Abdelaziz O, Graham S. Thermal charging performance of enhanced phase change material composites for thermal battery design. Int J Therml Sci. 2018;127:19-28.

[26] Jin H-Q, Fan L-W, Liu M-J, Zhu Z-Q, Yu Z-T. A pore-scale visualized study of melting heat transfer of a paraffin wax saturated in a copper foam: effects of the pore size. Int J Heat Mass Transfer. 2017;112:39-44.

[27] Xiao X, Zhang P, Li M. Preparation and thermal characterization of paraffin/metal foam composite phase change material. Appl Energy. 2013;112:1357-66.

[28] Weaver JA, Viskanta R. Melting of frozen, porous media contained in a horizontal or a vertical, cylindrical capsule. Int J Heat Mass Transfer. 1986;29:1943-51.

[29] Beckermann C, Viskanta R. Natural convection solid/liquid phase change in porous media. Int J Heat Mass Transfer. 1988;31:35-46.

[30] Zhao CY, Lu W, Tian Y. Heat transfer enhancement for thermal energy storage using metal foams embedded within phase change materials (PCMs). Sol Energy. 2010;84:1402-12.

[31] Chen Z, Gao D, Shi J. Experimental and numerical study on melting of phase change materials in metal foams at pore scale. Int J Heat Mass Transfer. 2014;72:646-

55.

[32] Jackson GR, Fisher T. Response of porous foams filled with phase change material under transient heating. 45th AIAA Thermophysics Conference, 2015. p. 2811.

[33] Fleming E, Wen S, Shi L, Da Silva AK. Experimental and theoretical analysis of an aluminum foam enhanced phase change thermal storage unit. Int J Heat Mass Transfer. 2015;82:273-81.

[34] Atal A, Wang Y, Harsha M, Sengupta S. Effect of porosity of conducting matrix on a phase change energy storage device. Int J Heat Mass Transfer. 2016;93:9-16.

[35] Zhang Z, He X. Three-dimensional numerical study on solid-liquid phase change within open-celled aluminum foam with porosity gradient. Appl Therm Eng. 2017;113:298-308.

[36] Zheng H, Wang C, Liu Q, Tian Z, Fan X. Thermal performance of copper foam/paraffin composite phase change material. Energy Convers Manage. 2018;157:372-81.

[37] Fukai J, Hamada Y, Morozumi Y, Miyatake O. Improvement of thermal characteristics of latent heat thermal energy storage units using carbon-fiber brushes: experiments and modeling. Int J Heat Mass Transfer. 2003;46:4513-25.

[38] Caliano M, Bianco N, Graditi G, Mongibello L. Analysis of a phase change material-based unit and of an aluminum foam/phase change material composite-based unit for cold thermal energy storage by numerical simulation. Appl Energy. 2019;256:113921.

[39] Yang X, Bai Q, Zhang Q, Hu W, Jin L, Yan J. Thermal and economic analysis of charging and discharging characteristics of composite phase change materials for cold storage. Appl Energy. 2018;225:585-99.

[40] Wang H, Wang F, Li Z, Tang Y, Yu B, Yuan W. Experimental investigation on the thermal performance of a heat sink filled with porous metal fiber sintered felt/paraffin composite phase change material. Appl Energy. 2016;176:221-32.

[41] Yang X, Wei P, Cui X, Jin L, He Y-L. Thermal response of annuli filled with metal foam for thermal energy storage: An experimental study. Appl Energy. 2019;250:1457-67.

[42] Al-Jethelah M, Ebadi S, Venkateshwar K, Tasnim SH, Mahmud S, Dutta A. Charging nanoparticle enhanced bio-based PCM in open cell metallic foams: An experimental investigation. Appl Therm Eng. 2019;148:1029-42.

[43] Cui HT. Experimental investigation on the heat charging process by paraffin filled with high porosity copper foam. Appl Therm Eng. 2012;39:26-8.

[44] Li WQ, Qu ZG, Zhang BL, Zhao K, Tao WQ. Thermal behavior of porous stainless-steel fiber felt saturated with phase change material. Energy. 2013;55:846-52.

[45] Diani A, Campanale M. Transient melting of paraffin waxes embedded in aluminum foams: Experimental results and modeling. Int J Therml Sci. 2019;144:119-28.

[46] Venkateshwar K, Ebadi S, Simha H, Mahmud S. Influence of Pore Density and Porosity on the Melting Process of Bio-Based Nano-Phase Change Materials Inside Open-Cell Metal Foam. J Therm Sci Eng Appl. 2019;11.

[47] Siahpush A, O'Brien J, Crepeau J. Phase Change Heat Transfer Enhancement Using Copper Porous Foam. J Heat Transfer. 2008;130.

[48] Yang J, Yang L, Xu C, Du X. Experimental study on enhancement of thermal energy storage with phase-change material. Appl Energy. 2016;169:164-76.

[49] Zhou D, Zhao CY. Experimental investigations on heat transfer in phase change materials (PCMs) embedded in porous materials. Appl Therm Eng. 2011;31:970-7.

[50] Cozzolino R, Chiappini D, Bella G. Experimental characterisation of a novel thermal energy storage based on open-cell copper foams immersed in organic phase change material. Energy Convers Manage. 2019;200:112101.

[51] Fan L-W, Jin H-Q. Local thermal nonequilibrium during melting of a paraffin filled in an open-cell copper foam: a visualized study at the pore-scale. J Heat Transfer. 2017;139:034505.

[52] Mancin S, Diani A, Doretti L, Hooman K, Rossetto L. Experimental analysis of phase change phenomenon of paraffin waxes embedded in copper foams. Int J Therml Sci. 2015;90:79-89.

[53] Wang Z, Zhang Z, Jia L, Yang L. Paraffin and paraffin/aluminum foam composite phase change material heat storage experimental study based on thermal management of Li-ion battery. Appl Therm Eng. 2015;78:428-36.

[54] Xiao X, Zhang P. Numerical and experimental study of heat transfer characteristics of a shell-tube latent heat storage system: Part I–Charging process. Energy. 2015;79:337-50.

[55] Yao Y, Wu H, Liu Z, Gao Z. Pore-scale visualization and measurement of paraffin melting in high porosity open-cell copper foam. Int J Therml Sci. 2018;123:73-85.

[56] Allen MJ, Bergman TL, Faghri A, Sharifi N. Robust heat transfer enhancement during melting and solidification of a phase change material using a combined heat pipe-metal foam or foil configuration. J Heat Transfer. 2015;137:102301.

[57] Rehman T-u, Ali HM. Experimental investigation on paraffin wax integrated with copper foam based heat sinks for electronic components thermal cooling. Int Commun Heat Mass. 2018;98:155-62.

[58] Baby R, Balaji C. Experimental investigations on thermal performance enhancement and effect of orientation on porous matrix filled PCM based heat sink.

Int Commun Heat Mass. 2013;46:27-30.

[59] Martinelli M, Bentivoglio F, Caron-Soupart A, Couturier R, Fourmigue J-F, Marty P. Experimental study of a phase change thermal energy storage with copper foam. Appl Therm Eng. 2016;101:247-61.

[60] Minkowycz WJ, Haji-Sheikh A, Vafai KF. On departure from local thermal equilibrium in porous media due to a rapidly changing heat source: the Sparrow number. Int J Heat Mass Transfer. 1999;42:3373-85.

[61] Agyenim F, Hewitt N, Eames P, Smyth M. A review of materials, heat transfer and phase change problem formulation for latent heat thermal energy storage systems (LHTESS). Renew Sustain Energy Rev. 2010;14:615-28.

[62] Allen MJ, Sharifi N, Faghri A, Bergman TL. Effect of inclination angle during melting and solidification of a phase change material using a combined heat pipe-metal foam or foil configuration. Int J Heat Mass Transfer. 2015;80:767-80.

[63] Yang X, Guo Z, Liu Y, Jin L, He Y-L. Effect of inclination on the thermal response of composite phase change materials for thermal energy storage. Appl Energy. 2019;238:22-33.

[64] Al-Abidi AA, Mat SB, Sopian K, Sulaiman MY, Mohammed AT. CFD applications for latent heat thermal energy storage: a review. Renew Sustain Energy Rev. 2013;20:353-63.

[65] Liu Q, Feng X-B, He Y-L, Lu C-W, Gu Q-H. Three-dimensional multiple-relaxation-time lattice Boltzmann models for single-phase and solid-liquid phase-change heat transfer in porous media at the REV scale. Appl Therm Eng. 2019;152:319-37.

[66] He Y-L, Liu Q, Li Q, Tao W-Q. Lattice Boltzmann methods for single-phase and solid-liquid phase-change heat transfer in porous media: A review. Int J Heat Mass Transfer. 2019;129:160-97.

[67] Ma Q, Chen Z, Liu H. Multiple-relaxation-time lattice Boltzmann simulation for flow, mass transfer, and adsorption in porous media. Phys Rev E. 2017;96:013313.

[68] Yang X, Bai Q, Guo Z, Niu Z, Yang C, Jin L, Lu TJ, et al. Comparison of direct numerical simulation with volume-averaged method on composite phase change materials for thermal energy storage. Appl Energy. 2018;229:700-14.

[69] Li X, Zhu Z, Xu Z, Ma T, Zhang H, Liu J, Wang X, et al. A three-dimensional pore-scale lattice Boltzmann model for investigating the supergravity effects on charging process. Appl Energy. 2019;254:113507.

[70] Kaviany M. Principles of heat transfer in porous media. Berlin: Springer; 1995.

[71] Hu X, Wan H, Patnaik SS. Numerical modeling of heat transfer in open-cell micro-foam with phase change material. Int J Heat Mass Transfer. 2015;88:617-26.

[72] Feng S, Shi M, Li Y, Lu TJ. Pore-scale and volume-averaged numerical simulations of melting phase change heat transfer in finned metal foam. Int J Heat Mass Transfer. 2015;90:838-47.

[73] Sundarram SS, Li W. The effect of pore size and porosity on thermal management performance of phase change material infiltrated microcellular metal foams. Appl Therm Eng. 2014;64:147-54.

[74] Yang J, Du X, Yang L, Yang Y. Numerical analysis on the thermal behavior of high temperature latent heat thermal energy storage system. Sol Energy. 2013;98:543-52.

[75] Xu Y, Li M-J, Zheng Z-J, Xue X-D. Melting performance enhancement of phase change material by a limited amount of metal foam: Configurational optimization and economic assessment. Appl Energy. 2018;212:868-80.

[76] Joseph DD, Nield DA, Papanicolaou G. Nonlinear equation governing flow in a saturated porous medium. Water Resour Res. 1982;18:1049-52.

[77] Nield DA, Bejan A. Convection in porous media. Berlin: Springer; 2006.

[78] Joshi V, Rathod MK. Thermal performance augmentation of metal foam infused phase change material using a partial filling strategy: An evaluation for fill height ratio and porosity. Appl Energy. 2019;253:113621.

[79] Hong Y, Ye W-B, Du J, Huang S-M. Solid-liquid phase-change thermal storage and release behaviors in a rectangular cavity under the impacts of mushy region and low gravity. Int J Heat Mass Transfer. 2019;130:1120-32.

[80] Fadl M, Eames PC. Numerical investigation of the influence of mushy zone parameter Amush on heat transfer characteristics in vertically and horizontally oriented thermal energy storage systems. Appl Therm Eng. 2019;151:90-9.

[81] Qu ZG, Li WQ, Tao WQ. Numerical model of the passive thermal management system for high-power lithium ion battery by using porous metal foam saturated with phase change material. Int J Hydrogen Energy. 2014;39:3904-13.

[82] Zhu F, Zhang C, Gong X. Numerical analysis on the energy storage efficiency of phase change material embedded in finned metal foam with graded porosity. Appl Therm Eng. 2017;123:256-65.

[83] Liu Z, Yao Y, Wu H. Numerical modeling for solid–liquid phase change phenomena in porous media: Shell-and-tube type latent heat thermal energy storage. Appl Energy. 2013;112:1222-32.

[84] Augspurger M, Udaykumar HS. A Cartesian grid solver for simulation of a phase-change material (PCM) solar thermal storage device. Numer Heat Tr B-Fund. 2016;69:179-96.

[85] Nithyanandam K, Pitchumani R. Computational Studies on Metal Foam and Heat Pipe Enhanced Latent Thermal Energy Storage. J Heat Transfer. 2014;136.

[86] Chen Z, Gu M, Peng D. Heat transfer performance analysis of a solar flat-plate collector with an integrated metal foam porous structure filled with paraffin. Appl Therm

Eng. 2010;30:1967-73.

[87] Žukauskas A. Heat Transfer from Tubes in Crossflow. In: Hartnett JP, Irvine TF, editors. Advances in Heat Transfer: Elsevier; 1972. p. 93-160.

[88] Sardari PT, Mohammed HI, Giddings D, walker GS, Gillott M, Grant D. Numerical study of a multiple-segment metal foam-PCM latent heat storage unit: Effect of porosity, pore density and location of heat source. Energy. 2019;189:116108.

[89] Churchill SW, Chu HHS. Correlating equations for laminar and turbulent free convection from a vertical plate. Int J Heat Mass Transfer. 1975;18:1323-9.

[90] Zhao Y, Zhao CY, Xu ZG, Xu HJ. Modeling metal foam enhanced phase change heat transfer in thermal energy storage by using phase field method. Int J Heat Mass Transfer. 2016;99:170-81.

[91] Srivatsa PVSS, Baby R, Balaji C. Numerical Investigation of PCM Based Heat Sinks with Embedded Metal Foam/Crossed Plate Fins. Numer Heat Tr A-Appl. 2014;66:1131-53.

[92] Kuwahara F, Shirota M, Nakayama A. A numerical study of interfacial convective heat transfer coefficient in two-energy equation model for convection in porous media. Int J Heat Mass Transfer. 2001;44:1153-9.

[93] Di Giorgio P, Iasiello M, Viglione A, Mameli M, Filippeschi S, Di Marco P, Andreozzi A, et al. Numerical Analysis of a Paraffin/Metal Foam Composite for Thermal Storage. Journal of Physics: Conference Series. 2017;796:012032.

[94] Yang X, Yu J, Guo Z, Jin L, He Y-L. Role of porous metal foam on the heat transfer enhancement for a thermal energy storage tube. Appl Energy. 2019;239:142-56.

[95] Mahdi JM, Nsofor EC. Melting enhancement in triplex-tube latent heat energy storage system using nanoparticles-metal foam combination. Appl Energy. 2017;191:22-34.

[96] Zhu F, Zhang C, Gong X. Numerical analysis and comparison of the thermal performance enhancement methods for metal foam/phase change material composite. Appl Therm Eng. 2016;109:373-83.

[97] Krishnan S, Murthy JY, Garimella SV. A two-temperature model for solid-liquid phase change in metal foams. J Heat Transfer. 2005;127:995-1004

[98] Tian Y, Zhao CY. A numerical investigation of heat transfer in phase change materials (PCMs) embedded in porous metals. Energy. 2011;36:5539-46.

[99] Yang J, Yang L, Xu C, Du X. Numerical analysis on thermal behavior of solid–liquid phase change within copper foam with varying porosity. Int J Heat Mass Transfer. 2015;84:1008-18.

[100] Lafdi K, Mesalhy O, Elgafy A. Graphite foams infiltrated with phase change materials as alternative materials for space and terrestrial thermal energy storage applications. Carbon. 2008;46:159-68.

[101] Xu Y, Ren Q, Zheng Z-J, He Y-L. Evaluation and optimization of melting performance for a latent heat thermal energy storage unit partially filled with porous media. Appl Energy. 2017;193:84-95.

[102] Li Q, Luo KH, Kang QJ, He YL, Chen Q, Liu Q. Lattice Boltzmann methods for multiphase flow and phase-change heat transfer. Prog Energy Combust Sci. 2016;52:62-105.

[103] Gao D, Chen Z. Lattice Boltzmann simulation of natural convection dominated melting in a rectangular cavity filled with porous media. Int J Therml Sci. 2011;50:493-501.

[104] McNamara GR, Zanetti G. Use of the Boltzmann equation to simulate lattice-gas automata. Phys Rev Lett. 1988;61:2332.

[105] Luo K, Yao F-J, Yi H-L, Tan H-P. Lattice Boltzmann simulation of convection

melting in complex heat storage systems filled with phase change materials. Appl Therm Eng. 2015;86:238-50.

[106] Zhao W, Zhang Y, Xu B, Li P, Wang Z, Jiang S. Multiple-Relaxation-Time Lattice Boltzmann Simulation of Flow and Heat Transfer in Porous Volumetric Solar Receivers. J Energ Resour-ASME. 2018;140:082003.

[107] Ren Q, Meng F, Guo P. A comparative study of PCM melting process in a heat pipe-assisted LHTES unit enhanced with nanoparticles and metal foams by immersed boundary-lattice Boltzmann method at pore-scale. Int J Heat Mass Transfer. 2018;121:1214-28.

[108] Guo Z, Zhao TS. Lattice Boltzmann model for incompressible flows through porous media. Phys Rev E. 2002;66:036304.

[109] Huo Y, Guo Y, Rao Z. Investigation on the thermal performance of phase change material/porous medium-based battery thermal management in pore scale. Int J Energ Res. 2019;43:767-78.

[110] Li X, Ma T, Liu J, Zhang H, Wang Q. Pore-scale investigation of gravity effects on phase change heat transfer characteristics using lattice Boltzmann method. Appl Energy. 2018;222:92-103.

[111] Liu Z, Wu H. Pore-scale study on flow and heat transfer in 3D reconstructed porous media using micro-tomography images. Appl Therm Eng. 2016;100:602-10.

[112] Liu Z, Wu H. Pore-scale modeling of immiscible two-phase flow in complex porous media. Appl Therm Eng. 2016;93:1394-402.

[113] d'Humières D, Shizgal BD. Rarefied gas dynamics: theory and simulations. Washington, DC: AIAA; 1992.

[114] Lallemand P, Luo LS. Theory of the lattice Boltzmann method: Dispersion, dissipation, isotropy, Galilean invariance, and stability. Phys Rev E. 2000;61:6546-62.

[115] Liu Q, He Y-L. Double multiple-relaxation-time lattice Boltzmann model for solid–liquid phase change with natural convection in porous media. Physica A. 2015;438:94-106.

[116] Liu Q, He Y-L, Li Q. Enthalpy-based multiple-relaxation-time lattice Boltzmann method for solid-liquid phase-change heat transfer in metal foams. Phys Rev E. 2017;96:023303.

[117] Li X, Zhu Z, Xu Z, Ma T, Zhang H, Liu J, Wang Q. Effect of supergravity on heat transfer characteristics of PCM with the pore-scale lattice Boltzmann method. Energy Procedia. 2019;158:4641-7.

[118] Peng Y, Chew YT, Shu C. Numerical simulation of natural convection in a concentric annulus between a square outer cylinder and a circular inner cylinder using the Taylor-series-expansion and least-squares-based lattice Boltzmann method. Phys Rev E. 2003;67:026701.

[119] Shi Y, Zhao TS, Guo ZL. Thermal lattice Bhatnagar-Gross-Krook model for flows with viscous heat dissipation in the incompressible limit. Phys Rev E. 2004;70:066310.

[120] Li Q, He YL, Wang Y, Tang GH. An improved thermal lattice boltzmann model for flows without viscous heat dissipation and compression work. Int J Mod Phys C. 2008;19:125-50.

[121] Jiaung WS, Ho JR, Kuo CP. Lattice Boltzmann method for the heat conduction problem with phase change. Numer Heat Tr B-Fund. 2001;39:167-87.

[122] Chatterjee D, Chakraborty S. An enthalpy-based lattice Boltzmann model for diffusion dominated solid–liquid phase transformation. Phys Lett A. 2005;341:320-30.

[123] Huber C, Parmigiani A, Chopard B, Manga M, Bachmann O. Lattice Boltzmann model for melting with natural convection. Int J Heat Fluid Flow. 2008;29:1469-80.

[124] Jany P, Bejan A. Scaling theory of melting with natural convection in an enclosure.

Int J Heat Mass Transfer. 1988;31:1221-35.

[125] Song W, Zhang Y, Li B, Fan X. A lattice Boltzmann model for heat and mass transfer phenomena with phase transformations in unsaturated soil during freezing process. Int J Heat Mass Transfer. 2016;94:29-38.

[126] Liu Q, He Y-L, Li D, Li Q. Non-orthogonal multiple-relaxation-time lattice Boltzmann method for incompressible thermal flows. Int J Heat Mass Transfer. 2016;102:1334-44.

[127] Liu Q, He Y-L, Li Q, Tao W-Q. A multiple-relaxation-time lattice Boltzmann model for convection heat transfer in porous media. Int J Heat Mass Transfer. 2014;73:761-75.

[128] Ren Q, He Y-L, Su K-Z, Chan CL. Investigation of the effect of metal foam characteristics on the PCM melting performance in a latent heat thermal energy storage unit by pore-scale lattice Boltzmann modeling. Numer Heat Tr A-Appl. 2017;72:745-64.

[129] Wu W, Zhang S, Wang S. A novel lattice Boltzmann model for the solid–liquid phase change with the convection heat transfer in the porous media. Int J Heat Mass Transfer. 2017;104:675-87.

[130] Mezrhab A, Amine Moussaoui M, Jami M, Naji H, Bouzidi Mh. Double MRT thermal lattice Boltzmann method for simulating convective flows. Phys Lett A. 2010;374:3499-507.

[131] Dubois F, Lin C-A, Tekitek MM. Anisotropic thermal lattice Boltzmann simulation of 2D natural convection in a square cavity. Comput Fluids. 2016;124:278-87.

[132] Du S, Li M-J, Ren Q, Liang Q, He Y-L. Pore-scale numerical simulation of fully coupled heat transfer process in porous volumetric solar receiver. Energy. 2017;140:1267-75.

[133] Zafari M, Panjepour M, Davazdah Emami M, Meratian M. Microtomography-based numerical simulation of fluid flow and heat transfer in open cell metal foams. Appl Therm Eng. 2015;80:347-54.

[134] Wang M, Pan N. Predictions of effective physical properties of complex multiphase materials. Mater Sci Eng R. 2008;63:1-30.

[135] Ma Q, Chen Z, Shi J, Li D. Lattice Boltzmann modeling of VOC desorption and diffusion in porous materials: VOC desorption and diffusion. Build Environ. 2014;72:145-53.

[136] Maier RS, Kroll DM, Bernard RS, Howington SE, Peters JF, Davis HT. Pore-scale simulation of dispersion. Phys Fluids. 2000;12:2065-79.

[137] Zhang H, Ge X, Ye H. Randomly mixed model for predicting the effective thermal conductivity of moist porous media. J Phys D: Appl Phys. 2005;39:220.